Received 5 June 2021; accepted 24 June 2021. Date of publication 30 June 2021; date of current version 14 July 2021.

Digital Object Identifier 10.1109/OJCOMS.2021.3093671

Performance Analysis of Energy Harvesting-Assisted Overlay Cognitive NOMA Systems With Incremental Relaying

ALOK KUMAR SHUKLA [1] (Graduate Student Member, IEEE), VIBHUM SINGH [1] (Graduate Student Member, IEEE), PRABHAT K. UPADHYAY [1] (Senior Member, IEEE), ABHINAV KUMAR [2] (Senior Member, IEEE), AND JULES M. MOUALEU [3] (Senior Member, IEEE)

[1]Department of Electrical Engineering, Indian Institute of Technology Indore, Indore 453552, India

[2]Department of Electrical Engineering, Indian Institute of Technology Hyderabad, Hyderabad 502285, India

[3]School of Electrical and Information Engineering, University of the Witwatersrand, Johannesburg 2000, South Africa

CORRESPONDING AUTHOR: P. K. UPADHYAY (e-mail: pkupadhyay@iiti.ac.in)

This work was supported by BRICS Multilateral R&D Project under Grant DST/IMRCD/BRICS/PILOTCALL2/LargEWiN/2018(G). The work of Prabhat K. Upadhyay was supported in part by the Project through the Visvesvaraya Ph.D. Scheme of Ministry of Electronics & Information Technology (MeitY), Government of India, being implemented by Digital India Corporation (formerly, Media Lab Asia). The work of Jules M. Moualeu was supported in part by the National Research Foundation (NRF) of South Africa under Grant 116018.

ABSTRACT In this paper, we analyze the performance of an energy harvesting (EH)-assisted overlay cognitive non-orthogonal multiple access (NOMA) system. The underlying system consists of a primary transmitter-receiver pair accompanied by an energy-constrained secondary transmitter (ST) with its intended receiver. Accordingly, ST employs a time switching (TS) based receiver architecture to harvest energy from radio-frequency signals of the primary transmissions, and thereby uses this energy to relay the primary information and to transmit its own information simultaneously using the NOMA principle. For this, we propose two cooperative spectrum sharing (CSS) schemes based on incremental relaying (IR) protocol using amplify-and-forward (AF) and decode-and-forward (DF) strategies, viz., CSS-IAF and CSS-IDF, and compare their performance with the competitive fixed relaying based schemes. The proposed IR-based schemes adeptly avail the degrees-of-freedom to boost the system performance. Thereby, considering the realistic assumption of the NOMA-based imperfect successive interference cancellation, we derive the expressions of outage probability for the primary and secondary networks under both CSS-IAF and CSS-IDF schemes subject to the Nakagami-m fading. In addition, we quantify the throughput and energy efficiency for the considered system. The obtained theoretical findings are finally validated through numerous analytical and simulation results to reveal the advantages of the proposed CSS schemes over the baseline direct link transmission and orthogonal multiple access schemes.

INDEX TERMS Amplify-and-forward, cognitive radio, decode-and-forward, energy harvesting, incremental relaying, non-orthogonal multiple access (NOMA), overlay spectrum sharing, simultaneous wireless information and power transfer (SWIPT).

I. INTRODUCTION

THE DEMAND for spectrum resources has proliferated with the recent developments in information and communication technologies. Thus, a key objective of the research community in the fifth-generation (5G) and beyond wireless networks is the enhancement

of the spectrum efficiency [1]. Among the existing techniques, non-orthogonal multiple access (NOMA) has been envisioned as a promising technology to attain higher spectral efficiency and massive connectivity for the future wireless networks [2]–[4]. One of the pivotal advantages of NOMA over traditional orthogonal multiple access (OMA) is to transmit multiple users' signals simultaneously in the same resource block (i.e., time/frequency/code domain) by exploiting the power domain multiplexing at the transmitter [5]. Thereby, the successive interference cancellation (SIC) is employed at the receiver to separate the multiplexed signals [6]–[8].

A. LITERATURE REVIEW

Recently, the NOMA technique has been commonly debated in the context of cognitive radio (CR), which is another potential technique for improving the spectrum efficiency [9]. In CR, a secondary user (SU) is allowed to use the spectrum licensed to the primary user (PU) by exploiting the underlay, overlay, or interweave spectrum sharing methodologies [10]. In the underlay approach, the SU is allowed to utilize the licensed spectrum concurrently with the PU, on condition that the interference caused by the SU is below a predefined threshold to satisfy the quality-of-service (QoS) of the PU [11]. In the overlay paradigm, both the PU and the SU share the same licensed spectrum for their signals transmission, and in exchange, the SU has to provide relay cooperation towards the PU on a priority basis [12]. On the other hand, in the interweave methodology, the SU opportunistically access the licensed spectrum while relying on the spectrum sensing towards the PU's activity [13]. Eventually, the incorporation of NOMA into CR, referred to as cognitive NOMA (CNOMA), has demonstrated a potential attribute of fulfilling the criteria of 5G wireless networks such as maximum throughput, broad connectivity, and low latency [14]. With the applicability of CNOMA, several research studies have been coordinated using the underlay [15]–[19] and overlay [20]–[25] approaches. Particularly, authors in [15] have investigated the outage performance of the large-scale underlay CNOMA network using stochastic geometry. The outage performance of SUs in underlay CNOMA using amplify-and-forward (AF) [16] and decode-and-forward (DF) [17] relaying protocols have been analyzed. Various relay selection schemes have been explored in [18] for an underlay CNOMA system operating with multiple DF relays. A cooperative underlay CNOMA-based coordinated direct and relay transmission has been investigated in [19]. In contrast to the underlay CNOMA, authors in [20], [21] have studied the overlay CNOMA model which deputes the secondary transmitter (ST) to act as a relay for the PU and also allows it to communicate with its secondary receivers (SRs) using the NOMA principle. In addition, authors in [22] have examined the outage performance of the PU and SU while comparing with the conventional OMA scheme. A clustering-based overlay spectrum sharing has been proposed by exploiting NOMA in coordinated direct and relay transmission in [23]. In [24], authors have incorporated the overlay CNOMA in hybrid satellite-terrestrial networks to facilitate multiple PUs, and thereby, have evaluated the outage probability (OP) expressions for the PUs and SU. An AF cooperative overlay CNOMA system has been analyzed in [25] assuming imperfect channel estimation and SIC. It needs to be acknowledged that the interference from the ST towards primary receiver (PR) is counteracted in the overlay CNOMA model in contrast to the underlay CNOMA. Moreover, the interference from PUs and stringent transmit power restrictions on SUs in underlay approach may limit the overall system performance and coverage. On the contrary, due to an increased diversity gain from the ST relaying cooperation, the outage performance of PU can be greatly improved in overlay CNOMA system. Furthermore, an overlay CNOMA model is of vital importance since it can bring network coverage even when the primary direct link is disrupted due to shadowing and obstacles.

On another front, the growth in greenhouse gas emissions has become a critical challenge in the development of future wireless communication networks. As per [26], the approximate annual demand of energy consumption for cellular networks is around 60 billion kW-h world-wide. Moreover, due to the exponential proliferation of wireless networks to support universal coverage and communication, this energy demand is explosively rising. Further, with the rapid growth of the Internet-of-Things (IoT) applications, this system energy consumption is further growing rapidly. Therefore, it is consequential to use energy efficiently or to harness the sustainable energy sources. Energy harvesting (EH) has emerged as a promising solution to improve energy efficiency and to extend lifetime of energy-constrained networks. Owing to the instability of harvesting energy from natural sources such as solar and wind, an alternative method has been explored to enable wireless devices scavenge energy from radio frequency (RF) signals [27]. Capitalizing on the fact that RF signals carry both information and energy, a simultaneous wireless information and power transfer (SWIPT) technique [28] can be utilized to address the aforementioned concerns in wireless networks. This technique allows the wireless devices to harvest energy from the ambient RF sources and to transmit the information simultaneously [29]. To facilitate SWIPT in wireless networks, two practical receiver architectures viz., power splitting (PS) and time switching (TS) have been investigated [30]. In PS-based SWIPT, the receiver node splits the power between EH and information transmission (IT) phases, whereas in TS-based SWIPT, time is switched between EH and IT phases. The SWIPT technique finds useful applications in device-to-device (D2D) networks, small cell (picocell and femtocell) networks, and wireless sensor networks (e.g., for a smart city deployment), where the devices generally do not have a dedicated spectrum for their communication, and they are equipped with power-constrained low-cost transceiver hardware. Moreover, RF-based EH systems can be built cheaply in small dimensions, which could be a remarkable advantage

in the manufacturing of small and low cost devices such as the SU nodes. A SWIPT-enhanced overlay spectrum sharing system has been recently studied in [31] by considering a piece-wise linear EH model which relies on a TS-based receiver architecture.

By incorporating SWIPT into CNOMA, a more spectral and energy efficient wireless network is expected to be framed with a sustainable environment. There have been diverse research works done by considering SWIPT into CNOMA [32]–[36]. Authors in [32] have investigated a cooperative multiple-input-single-output SWIPT NOMA protocol, where a strong NOMA user serves as an EH relay and assists a weak NOMA user by using the PS protocol. The work in [33] has studied an underlay non-linear EH-assisted CNOMA system to improve the spectral efficiency and secrecy energy efficiency. A SWIPT-enhanced overlay CNOMA system has been studied in [34] to achieve the maximal throughput for the secondary network. Authors in [35] have studied the energy efficiency optimization problem for both the underlay and overlay CNOMA with EH. The outage performance of cooperative CNOMA networks with SWIPT using DF relaying has been investigated in [36], where cognitive relay harvests the transmission power from the ST by exploiting the PS scheme using the fixed power allocation based NOMA protocol. A very recent work in [37] conducted the performance analysis for the power beacon-assisted wireless powered NOMA by enabling the co-existence of cellular network with the IoT communication.

B. MOTIVATION AND CONTRIBUTIONS

The aforementioned works on SWIPT-enabled CNOMA networks follow the conventional fixed relaying (FR) strategy which impels the ST to incorporate the relaying operation even when the PR is able to decode its signal through the primary direct link (DL), which is not at all an efficient way of utilizing the spectrum. Moreover, they have assumed the ideal case of perfect SIC (pSIC) for the performance investigation. However, the pSIC is difficult to realize in practice, owing to the many implementation issues, such as complexity scaling and error propagation [38]. Consequently, these critical factors will lead to an error in decoding, causing residual interference signal (IS). Thereby, the effects of imperfect SIC (ipSIC) [39] may pose limitations on the capacity of the SWIPT-based CNOMA network. While few recent works have considered the impact of ipSIC [22], [25], [40] on the performance evaluation of CNOMA networks, they have not explored the potential features of SWIPT. To the best of authors' knowledge, no work has yet looked into the comprehensive performance analysis of SWIPT-enabled CNOMA networks under the impacts of both the ipSIC and pSIC situations. Note that such analyses are important to perceive the repercussion of ipSIC/pSIC on the practical design of CNOMA networks integrated with the EH technique for a more sustainable communication in 5G environments.

Motivated by the prior research studies, in this paper, we analyze the performance of an EH-assisted overlay CNOMA (EH-OCNOMA) system[1] by adopting an incremental relaying (IR) protocol under the impacts of ipSIC/pSIC situations. Specifically, we consider a downlink communication scenario wherein a primary transmitter (PT) communicates to a PR in cooperation with an energy-constrained ST accessing spectrum for its own communication to an SR. The ST employs a TS-based receiver architecture[2] to harvest energy from RF signals of the primary transmissions. Further, it can act as an AF/DF relay and uses the harvested energy to forward the primary signal and to transmit its own signal simultaneously using the NOMA principle. Importantly, the proposed IR protocol invokes secondary relay cooperation adaptively, depending on the limited feedback mechanism from the PU. It can thus proficiently utilize the available degrees-of-freedom to improve the system performance of EH-OCNOMA. The major contributions of the paper are emphasized as follows.

- We propose two EH-based cooperative spectrum sharing (CSS) schemes based on the IR protocol using the AF and DF relaying strategies, namely CSS-IAF and CSS-IDF, and compare their performance with the competitive FR-based schemes. We also discuss the DL transmission (DLT) scheme as a baseline to compare with the performance of CSS schemes for the considered EH-OCNOMA system. Further, we portray the relative performance advantages of CSS with NOMA over its OMA counterpart.
- Based on the received signal-to-noise ratios (SNRs) and signal-to-interference-plus-noise ratios (SINRs), we extensively analyze the outage performance of CSS-IAF and CSS-IDF schemes by deriving the OP expressions of the primary and secondary networks under the ipSIC/pSIC situations over a Nakagami-m fading[3] environment.
- To garner further insight, we also deduce the expressions of system throughput and energy efficiency for the considered EH-OCNOMA system.
- Finally, for the effective design of the proposed EH-OCNOMA system, we provide an insight into the NOMA power allocation factor to explore the spectrum sharing opportunities.

C. ORGANIZATION

The rest of the paper is organized as follows. Section II illustrates the system model and the proposed IR protocol

1. The considered EH-OCNOMA system comprises of the power-constrained low-cost SU nodes, capturing the application scenarios of device-to-device (D2D) networks, small cell (picocell and femtocell) networks, and wireless sensor networks, which generally do not have a dedicated spectrum for their communication.

2. In contrast to PS-based receiver, the TS-based receiver is simpler to implement (using hardware with simple switching circuits) and more suitable for low-cost devices [41].

3. The Nakagami-m fading model represents a general distribution wherein various fading environments, i.e., severe, light or no fading, can be modeled [42]. Moreover, it gives the best fit of the statistical characteristics of a land mobile system, complex environments and ionospheric radio links.

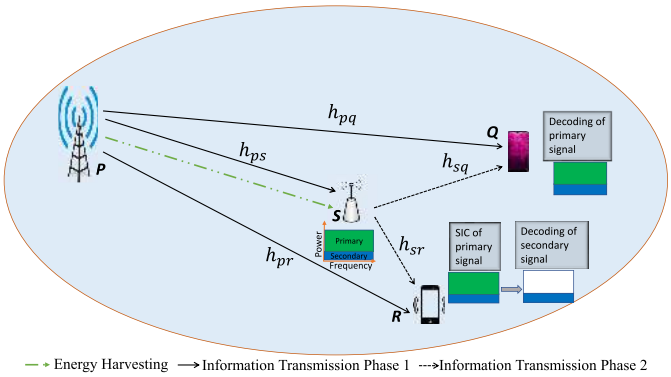

FIGURE 1. System model.

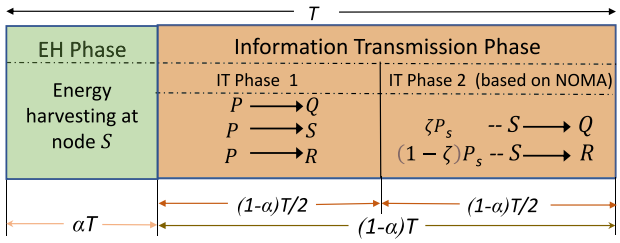

FIGURE 2. Transmission Block Structure for EH and IT phase.

for the EH-OCNOMA system, while deriving the end-to-end SNRs/SINRs for the primary and secondary networks. Section III investigates the performance of the primary network by evaluating the analytical expressions of the OP for the DLT, CSS-IAF, and CSS-IDF schemes. The OP expressions of the secondary network, while considering both the ipSIC and pSIC situations, have been evaluated in Section IV. The system throughput and the energy efficiency expressions for the proposed EH-OCNOMA system are presented in Section V. Section VI portrays the results and discussions, followed by some concluding remarks in Section VII. Moreover, the proofs of theorems/lemmas used in this paper are included in the Appendices.

Mathematical Functions Notations: $\mathcal{CN}(0, N_o)$ represents the complex Gaussian distribution with mean zero and variance N_o. $f_X(\cdot)$ and $F_X(\cdot)$ designate the probability density function (PDF) and the cumulative distribution function (CDF) of a random variable X, respectively. $\mathbb{E}[\cdot]$ denotes the expectation and $\binom{p}{q} = \frac{p!}{q!(p-q)!}$ implies the binomial coefficient. Further, $\mathcal{K}_v(\cdot)$ expresses the modified Bessel function of the second kind [43, eq. (8.432.6)], whereas $\Gamma(\cdot)$ and $\Upsilon(\cdot,\cdot)$ denote the complete Gamma function and lower incomplete Gamma function, as given in [43, eqs. (8.310.1) and (8.350.1)], respectively.

II. SYSTEM MODEL AND PROTOCOL DESCRIPTION

This section first provides a detailed description of the EH-OCNOMA system model and thereafter presents the end-to-end SINR/SNR expressions for the AF/DF relaying strategies, followed by elaborating the proposed IR protocol for the considered system.

A. SYSTEM MODEL

As depicted in Fig. 1, we consider an EH-OCNOMA system where a primary network coexists with a secondary network. The primary network comprises of a transmitter node P with its corresponding receiver node Q, whereas the secondary network includes an energy-constrained ST node S and SR node R. Herewith, node P establishes a communication directly with node Q. Although a primary DL between node P and node Q is supposed to exist, node P may still seek the ST's cooperation to exploit the diversity benefits. As an incentive for the cooperation with the primary network, the secondary network accesses the licensed spectrum of the primary network. Since S is an energy-constrained node, it first harvests energy from the received RF signal and then splits the corresponding harvested power to relay the primary signal and to transmit its own signal simultaneously using the NOMA principle. For this, it employs a TS-based receiver architecture, as shown in Fig. 2. Herein, the transmission block duration is divided into two phases of durations αT and $(1-\alpha)T$, with $\alpha \in (0,1)$ being the TS parameter. The first phase of duration αT corresponds to an EH phase, wherein the ST node S harvests the energy using the received RF signal from node P, and utilizes this energy further to broadcast the amalgamated signal in the second phase of duration, i.e., IT phase. The duration $(1-\alpha)T$ is further subdivided into two IT phases to establish the overall communication. It is assumed that all the nodes are equipped with single antenna and operate in half-duplex mode. All the channels are assumed to follow block fading, which means they remain unchanged for a particular block and may change for the subsequent block transmissions independently. Further, all the links are subject to independent Nakagami-m fading and the channel gain from node i to node j is represented by h_{ij}, where $i \in \{p, s\}$ and $j \in \{q, s, r\}$ with $i \neq j$. All the receiving nodes are assumed to be inflicted by the additive white Gaussian noise (AWGN), i.e., modelled as $\mathcal{CN}(0, N_o)$.

B. EH PHASE

During αT duration, node S harvests energy[4] from the transmitted RF signal through node P, which can be given by

$$E_s = \Theta P_p |h_{ps}|^2 \alpha T, \tag{1}$$

where P_p is the transmit power at node P and Θ ($0 < \Theta \leq 1$) is the energy conversion efficiency that relies on the rectification process and the associated EH circuitry [44]. Consequently, the transmit power at node S over the time $(1-\alpha)T/2$ can be obtained as

$$P_s = \frac{E_s}{(1-\alpha)T/2} = \frac{2\alpha\Theta P_p |h_{ps}|^2}{1-\alpha} = \beta P_p |h_{ps}|^2, \tag{2}$$

4. Herein, we consider a linear EH model for analytical tractability, as followed in many previous works [32]–[36]. A non-linear EH model [45] would however be more practical and may be tackled in the future work. Nevertheless, our present results can be treated as a benchmark for the futuristic design.

where $\beta = \frac{2\alpha\Theta}{1-\alpha}$. Hereby, the overall communication takes place in two IT phases, as discussed in the following subsection.

C. IT PHASE

During the first IT phase, node P transmits a primary signal x_p towards node Q, complying with $\mathbb{E}[|x_p|^2] = 1$, which is also received by the secondary nodes S and R. Thus, the received signal at node i, with $i \in \{q, s, r\}$, can be expressed as

$$y_{pi} = \sqrt{P_p} h_{pi} x_p + n_{pi}, \tag{3}$$

where n_{pi} is the AWGN term. Accordingly, the resulting SNR at node i through the DL can be written as

$$\gamma_{pi}^{\mathrm{DL}} = \eta_p |h_{pi}|^2, \tag{4}$$

with $\eta_p = \frac{P_p}{N_o}$ represents the transmit SNR at node P.

In what follows, we discuss the AF and DF based relaying strategies and thereby obtain the associated SINR expressions.

1) AF RELAYING

During the second IT phase, node S amplifies the received primary signal y_{ps} and superimposes with its own information signal x_s to generate a combined signal x_s^{AF} by exploiting the NOMA principle. This superimposed signal x_s^{AF} is further broadcasted towards nodes Q and R. For this, the harvested power P_s is divided such that ζP_s power is utilized to forward the signal y_{ps} and remaining power $(1-\zeta)P_s$ is used in transmitting the signal x_s, where $\zeta \in (0,1)$ signifies the NOMA-based power allocation parameter. Due to the higher priority of the primary network, more power is allocated to node Q, resulting in $\zeta \in (0.5,1)$. As such, the transmitted signal by the node S is given by

$$x_s^{\mathrm{AF}} = \sqrt{\zeta P_s}\mathcal{G} y_{ps} + \sqrt{(1-\zeta)P_s} x_s, \tag{5}$$

where the variable gain relaying amplification factor $\mathcal{G}$ at the AF-based relay can be expressed [46] as $\mathcal{G} = \sqrt{\frac{1}{P_p|h_{ps}|^2+N_o}}$, which can be further approximated as $\mathcal{G} \approx \sqrt{\frac{1}{P_p|h_{ps}|^2}}$ for analytical simplicity [31], [47]. Such approximation yields very accurate results over the entire region of operating SNR. Hereafter, the received signal at node j, where $j \in \{q, r\}$, can be expressed as

$$y_{sj}^{\mathrm{AF}} = h_{sj} x_s^{\mathrm{AF}} + n_{sj}, \tag{6}$$

with n_{sj} as the AWGN term. Consequently, the end-to-end SINR at node Q via the relay link can be obtained as

$$\gamma_{psq}^{\mathrm{AF}} = \frac{\zeta \gamma_{ps} \beta |h_{sq}|^2}{(1-\zeta)\gamma_{ps}\beta|h_{sq}|^2 + \zeta\beta|h_{sq}|^2 + 1}, \tag{7}$$

where $\gamma_{ps} = \eta_p |h_{ps}|^2$ which is same as $\gamma_{ps}^{\mathrm{DL}}$ in (4) and used invariably in the subsequent analysis. With the maximal-ratio-combining (MRC) method, node Q can thus combine the two copies of the primary signal, one from the first IT phase (through DLT) and other from the second IT phase (through relay cooperation).

On the other hand, after receiving the superposed NOMA signal at node R, the SR decodes its own signal x_s and discards the primary signal component x_p through SIC operation, while considering the primary component as an interference to the secondary node. For this, SR first decodes the primary signal x_p while treating the secondary signal x_s as noise. Accordingly, the SINR at node R can be given by

$$\gamma_{psr \to x_p}^{\mathrm{AF}} = \frac{\zeta \gamma_{ps} \beta |h_{sr}|^2}{(1-\zeta)\gamma_{ps}\beta|h_{sr}|^2 + \zeta\beta|h_{sr}|^2 + 1}. \tag{8}$$

Note that in the first phase of IT, the primary signal x_p has also been received at node R from node P directly. So, the MRC method is employed at node R to combine the received primary signal components in the first and second phases of IT.

Thereafter, SR decodes its own signal x_s by eliminating x_p from y_{sr}^{AF}. However, in practice, there may be some decoding errors owing to the imperfection in executing the SIC operation. Accordingly, a residual interference is assumed to exist, leading to an ipSIC term. Thus, after the ipSIC, the end-to-end SINR at node R can be provided as

$$\gamma_{psr}^{\mathrm{AF}} = \frac{(1-\zeta)\gamma_{ps}\beta|h_{sr}|^2}{\zeta\beta|h_{sr}|^2 + \tau\zeta\beta\gamma_{ps}|h_R|^2 + 1}, \tag{9}$$

where $\tau = 0$ and $\tau = 1$ imply the respective cases of pSIC and ipSIC, h_R is the residual IS channel coefficient at node R and is subject to Nakagami-m fading [48] with its corresponding fading severity parameter m_R and average channel power gain Ω_R.

2) DF RELAYING

In this relaying strategy, during the second IT phase, node S facilitates the DF-based relaying and makes an effort to decode the primary signal x_p. On successful decoding of the primary signal x_p at node S, it combines x_p with its own signal x_s to generate a superimposed signal x_s^{DF} as per the NOMA principle. Hence, the signal transmitted by node S is given by

$$x_s^{\mathrm{DF}} = \sqrt{\zeta P_s} x_p + \sqrt{(1-\zeta)P_s} x_s. \tag{10}$$

Hereafter, the received signal at node j, where $j \in \{q, r\}$, can be expressed as

$$y_{sj} = h_{sj} x_s^{\mathrm{DF}} + n_{sj}. \tag{11}$$

Consequently, the resultant SINR expression at node Q, based on (10) and (11), can be represented as

$$\gamma_{sq}^{\mathrm{DF}} = \frac{\zeta\beta\gamma_{ps}|h_{sq}|^2}{(1-\zeta)\gamma_{ps}\beta|h_{sq}|^2 + 1}. \tag{12}$$

Further, based on (10) and (11), the equivalent SINR at node R to decode the primary signal x_p can be obtained as

$$\gamma_{sr \to x_p}^{\mathrm{DF}} = \frac{\zeta\beta\gamma_{ps}|h_{sr}|^2}{(1-\zeta)\beta\gamma_{ps}|h_{sr}|^2 + 1}, \tag{13}$$

whereas, the resultant SINR at R to decode its own signal x_s can be provided as

$$\gamma_{sr}^{\mathrm{DF}} = \frac{(1-\zeta)\beta\gamma_{ps}|h_{sr}|^2}{\tau\beta\zeta\gamma_{ps}|h_R|^2+1}. \tag{14}$$

On the other hand, if node S fails to decode the primary signal x_p in the first IT phase, it will proceed with non-cooperation mode and transmit its own signal only to node R during the second IT phase, whereas, the PR node Q follows only the transmission through DL in the first IT phase.

D. PROPOSED IR PROTOCOL

In this protocol, the relaying cooperation is adeptly executed by the ST node S based on the successful or unsuccessful decoding of the primary signal x_p at node Q in the first IT phase. Importantly, the relaying cooperation is invoked depending on the success/failure of the DL ($P \to Q$) transmission. Consequently, the mutual information of the DLT can be written as

$$\mathcal{I}_{pq} = \log_2\left(1+\gamma_{pq}^{\mathrm{DL}}\right). \tag{15}$$

If node Q can successfully decode the information signal from node P, i.e., $\mathcal{I}_{pq} \geq R_p$, where R_p is a target threshold rate, it acknowledges the cooperative node S by sending an error-free one-bit feedback[5] that the relaying cooperation is not required. Accordingly, all the harvested power at node S can be utilized for its own information transmission towards the node R. Therefore, the secondary network's performance can be improved.

For the non-cooperation case (i.e., no relaying required), the signal transmitted by node S can be given as

$$x_s^{\mathrm{noc}} = \sqrt{P_s}x_s. \tag{16}$$

Thus, the signal received at node R from S can be expressed as

$$y_{sr}^{\mathrm{noc}} = h_{sr}x_s^{\mathrm{noc}} + n_{sr}. \tag{17}$$

Hereby, using (16) and (17), the resultant SNR expression at node R is given as

$$\gamma_{sr}^{\mathrm{noc}} = \beta\gamma_{ps}|h_{sr}|^2. \tag{18}$$

On the contrary, if node Q is unable to decode the information signal from node P in the first IT phase, i.e., if $\mathcal{I}_{pq} < R_p$, it sends a negative feedback to S. Thus, the relaying cooperation from ST is evoked and further IT operation follows either the AF or the DF relaying protocol. However, in the case of DF relaying, if the primary signal x_p could not be decoded at node S after the first IT phase, node S can utilize all its harvested power in transmitting its own information. Hence, the equivalent SNR expression at node R can be given by (18).

For the subsequent analysis, we refer the CSS schemes based on IR protocol using AF and DF relaying as CSS-IAF and CSS-IDF, respectively. The proposed IR protocol is depicted as a flowchart in Fig. 3.

III. OUTAGE PERFORMANCE OF PRIMARY NETWORK

In this section, the expressions for the OP of the primary network are derived under two transmission schemes, i.e., DLT and CSS (with IAF and IDF relaying strategies).

To proceed with the analysis, we first present the statistics of the underlying fading channels. As the pertinent links are subject to Nakagami-m fading, the PDF and CDF of $|h_{ij}|^2$, for $i \in \{p, s\}$ and $j \in \{q, s, r\}$ with $i \neq j$, can be, respectively, given by

$$f_{|h_{ij}|^2}(x) = \left(\frac{m_{ij}}{\Omega_{ij}}\right)^{m_{ij}} \frac{x^{m_{ij}-1}}{\Gamma\left(m_{ij}\right)} \mathrm{e}^{-\frac{m_{ij}}{\Omega_{ij}}x} \tag{19}$$

and

$$F_{|h_{ij}|^2}(x) = \frac{1}{\Gamma(m_{ij})}\Upsilon\left(m_{ij}, \frac{m_{ij}}{\Omega_{ij}}x\right), \tag{20}$$

where Ω_{ij} is the average power and m_{ij} is the fading severity parameter. Hereafter, we consider Nakagami-m channels with integer-valued fading parameters for analytical simplicity. Note that an integer-valued Nakagami-m fading model is widely adopted in literature since, in practice, the measurement accuracy of the underlying channel is typically of integer order [51]. However, the performance analysis can also be taken up for the non-integer case as followed in [52].

A. DLT SCHEME

We consider a DLT scheme which provides communication solely through the DL, i.e., without cooperation of the relay link. Basically, this scheme is examined as a benchmark to compare its performance with the proposed CSS scheme. As such, for a pre-defined target rate R_p, the OP of the primary network using the DLT scheme can be expressed as

$$P_{\mathrm{out}}^{\mathrm{DL}}(R_p) = \Pr\left[\log_2\left(1+\gamma_{pq}^{\mathrm{DL}}\right) < R_p\right], \tag{21}$$

which can be re-expressed as

$$P_{\mathrm{out}}^{\mathrm{DL}}(R_p) = \Pr\left[\gamma_{pq}^{\mathrm{DL}} < \gamma_p'\right] = F_{\gamma_{pq}^{\mathrm{DL}}}\left(\gamma_p'\right), \tag{22}$$

where $\gamma_p' = 2^{R_p} - 1$. Now, (22) requires the evaluation of the CDF $F_{\gamma_{pq}^{\mathrm{DL}}}(\gamma_p')$, which can be obtained using (20) as

$$F_{\gamma_{pq}^{\mathrm{DL}}}(\gamma_p') = \frac{1}{\Gamma(m_{pq})}\Upsilon\left(m_{pq}, \frac{m_{pq}}{\Omega_{pq}\eta_p}\gamma_p'\right). \tag{23}$$

B. CSS SCHEME

Herein, we appraise the outage performance of the primary network for the considered EH-OCNOMA with the CSS-IAF and CSS-IDF schemes as described in Section II.

5. The feedback/acknowledge time is considered to be small in contrast to the information processing time [49], [50]. It is worth noting that such feedback is transmitted over a separate low-bandwidth error-free channel, resulting in minimal delay.

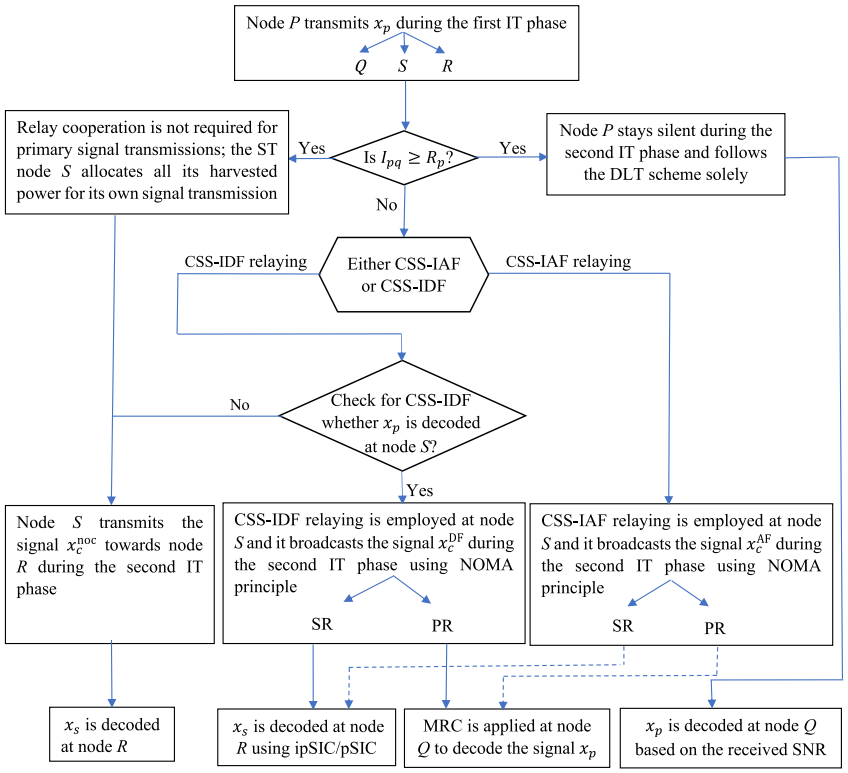

FIGURE 3. Flow chart for the proposed IR protocol.

1) CSS WITH IAF RELAYING (CSS-IAF)

For a given target rate R_p, the OP of the primary network for CSS-IAF scheme can be formulated as

$$P_{\text{out}}^{\text{AF}}(R_p) = \Pr\left[\gamma_{pq}^{\text{DL}} < \gamma_p', \gamma_{pq}^{\text{DL}} + \gamma_{psq}^{\text{AF}} < \gamma_p\right], \quad (24)$$

where $\gamma_p = 2^{\frac{2R_p}{1-\alpha}} - 1$. Further, $P_{\text{out}}^{\text{AF}}(R_p)$ in (24) can be expressed as

$$\begin{aligned} P_{\text{out}}^{\text{AF}}(R_p) &= \Pr\left[\gamma_{pq}^{\text{DL}} < \min\left(\gamma_p - \gamma_{psq}^{\text{AF}},\ \gamma_p'\right)\right] \\ &= \underbrace{\Pr\left[\gamma_{pq}^{\text{DL}} < \gamma_p',\ \gamma_p' < \gamma_p - \gamma_{psq}^{\text{AF}}\right]}_{I_1} \\ &\quad + \underbrace{\Pr\left[\gamma_{pq}^{\text{DL}} < \gamma_p - \gamma_{psq}^{\text{AF}},\ \gamma_p' \geq \gamma_p - \gamma_{psq}^{\text{AF}}\right]}_{I_2}. \end{aligned} \quad (25)$$

To derive the OP expression in (25), we have to evaluate the two probability terms I_1 and I_2. Hereby, we first evaluate the probability term I_1 as

$$\begin{aligned} I_1 &= \Pr\left[\gamma_{pq}^{\text{DL}} < \gamma_p',\ \gamma_{psq}^{\text{AF}} < \gamma_p - \gamma_p'\right] \\ &= F_{\gamma_{pq}^{\text{DL}}}(\gamma_p')\, F_{\gamma_{psq}^{\text{AF}}}\left(\gamma_p - \gamma_p'\right), \end{aligned} \quad (26)$$

where the multiplication of individual CDF terms results from the statistical independence between the two events. Now, (26) requires the evaluation of $F_{\gamma_{psq}^{\text{AF}}}(\gamma_p - \gamma_p')$, which can be derived as follows in Theorem 1.

Theorem 1: The CDF $F_{\gamma_{psq}^{\text{AF}}}(x)$ under Nakagami-m fading can be given by

$$F_{\gamma_{psq}^{\text{AF}}}(x) = \begin{cases} 1, & \text{if } x \geq \frac{\zeta}{1-\zeta}, \\ \phi_1(x), & \text{if } x < \frac{\zeta}{1-\zeta}, \end{cases} \quad (27)$$

where $\phi_1(x)$ is given as

$$\begin{aligned} \phi_1(x) = 1 - &\sum_{k=0}^{m_{ps}-1} \sum_{j=0}^{k} \frac{2}{k!} \left(\frac{T_0 x}{\theta_x}\right)^k e^{-\left(\frac{T_0 x \zeta \beta}{\theta_x}\right)} \left(\frac{m_{sq}}{\Omega_{sq}}\right)^{m_{sq}} \\ &\times \frac{1}{\Gamma(m_{sq})} \binom{k}{j} (\zeta\beta)^j \left(\frac{T_0 x \Omega_{sq}}{\theta_x m_{sq}}\right)^{\frac{m_{sq}+j-k}{2}} \\ &\times \mathcal{K}_{m_{sq}+j-k}\left(2\sqrt{\frac{T_0 x m_{sq}}{\theta_x \Omega_{sq}}}\right), \end{aligned} \quad (28)$$

with $T_0 = \frac{m_{ps}}{\Omega_{ps}\eta_p\beta}$ and $\theta_x = \zeta - (1-\zeta)x$.

Proof: See Appendix A. ■

It is noteworthy that the condition $x < \frac{\zeta}{1-\zeta}$ in (27) makes the CSS effective through the IAF relaying scheme, otherwise the value of the CDF $F_{\gamma_{psq}^{\text{AF}}}(x)$ becomes unity. This phenomenon is referred to as relay cooperation ceiling (RCC), and hereby, the primary communication solely follows the DLT scheme. By substituting (23) and (27) (with $x = \gamma_p - \gamma_p'$) into (26), one can obtain I_1.

Next, we evaluate the probability term I_2 as

$$\begin{aligned} I_2 &= \Pr\left[\gamma_{psq}^{\text{AF}} < \gamma_p - \gamma_{pq}^{\text{DL}},\ \gamma_{psq}^{\text{AF}} \geq \gamma_p - \gamma_p'\right] \\ &= \int_{\gamma_p - \gamma_p'}^{\gamma_p - y} \int_0^{\gamma_p} f_{\gamma_{psq}^{\text{AF}}}(x) f_{\gamma_{pq}^{\text{DL}}}(y)\, dx dy \end{aligned}$$

$$= \int_0^{\gamma_p} F_{\gamma_{psq}^{\mathrm{AF}}}(\gamma_p - y) f_{\gamma_{pq}^{\mathrm{DL}}}(y)dy - \int_0^{\gamma_p} F_{\gamma_{psq}^{\mathrm{AF}}}\left(\gamma_p - \gamma_p'\right) f_{\gamma_{pq}^{\mathrm{DL}}}(y)dy. \quad (29)$$

Using the CDF $F_{\gamma_{psq}^{\mathrm{AF}}}(x)$ into (29), it is intricate to get a closed-form solution for I_2. Hence, by applying an M-step staircase approximation approach [53] for the involved triangular integral region in (29), I_2 can be expressed as

$$I_2 \approx \sum_{i=0}^{M-1} \left\{ F_{\gamma_{pq}^{\mathrm{DL}}}\left(\frac{i+1}{M}\gamma_p\right) - F_{\gamma_{pq}^{\mathrm{DL}}}\left(\frac{i}{M}\gamma_p\right) \right\} \times F_{\gamma_{psq}^{\mathrm{AF}}}\left(\frac{M-i}{M}\gamma_p\right) - F_{\gamma_{psq}^{\mathrm{AF}}}(\gamma_p - \gamma_p')F_{\gamma_{pq}^{\mathrm{DL}}}(\gamma_p). \quad (30)$$

Finally, after inserting the expressions of I_1 and I_2 into (25), the analytical expression of $P_{\mathrm{out}}^{\mathrm{AF}}(R_p)$ can be obtained. As such, relying on the conditions on the threshold γ_p using (27), $P_{\mathrm{out}}^{\mathrm{AF}}(R_p)$ can be expressed for the following cases:

- When $\gamma_p < \frac{\zeta}{1-\zeta}$,

$$P_{\mathrm{out}}^{\mathrm{AF}}(R_p) \triangleq P_1(R_p) = F_{\gamma_{pq}^{\mathrm{DL}}}\left(\gamma_p'\right) F_{\gamma_{psq}^{\mathrm{AF}}}\left(\gamma_p - \gamma_p'\right) + \sum_{i=0}^{M-1} \left\{ F_{\gamma_{pq}^{\mathrm{DL}}}\left(\frac{i+1}{M}\gamma_p\right) - F_{\gamma_{pq}^{\mathrm{DL}}}\left(\frac{i}{M}\gamma_p\right) \right\} \times F_{\gamma_{psq}^{\mathrm{AF}}}\left(\frac{M-i}{M}\gamma_p\right) - F_{\gamma_{psq}^{\mathrm{AF}}}(\gamma_p - \gamma_p')F_{\gamma_{pq}^{\mathrm{DL}}}(\gamma_p). \quad (31)$$

- When $\frac{\zeta}{1-\zeta} \le \gamma_p < \frac{\zeta}{1-\zeta} + \gamma_p'$,

$$P_{\mathrm{out}}^{\mathrm{AF}}(R_p) \triangleq P_2(R_p) = F_{\gamma_{pq}^{\mathrm{DL}}}\left(\gamma_p'\right) F_{\gamma_{psq}^{\mathrm{AF}}}\left(\gamma_p - \gamma_p'\right) + \sum_{i=0}^{M-1} \left\{ F_{\gamma_{pq}^{\mathrm{DL}}}\left(\frac{i+1}{M}\gamma_p\right) - F_{\gamma_{pq}^{\mathrm{DL}}}\left(\frac{i}{M}\gamma_p\right) \right\} - F_{\gamma_{psq}^{\mathrm{AF}}}\left(\gamma_p - \gamma_p'\right)F_{\gamma_{pq}^{\mathrm{DL}}}(\gamma_p). \quad (32)$$

- When $\gamma_p \ge \frac{\zeta}{1-\zeta} + \gamma_p'$,

$$P_{\mathrm{out}}^{\mathrm{AF}}(R_p) \triangleq P_3(R_p) = F_{\gamma_{pq}^{\mathrm{DL}}}\left(\gamma_p'\right) - F_{\gamma_{pq}^{\mathrm{DL}}}(\gamma_p) + \sum_{i=0}^{M-1} \left\{ F_{\gamma_{pq}^{\mathrm{DL}}}\left(\frac{i+1}{M}\gamma_p\right) - F_{\gamma_{pq}^{\mathrm{DL}}}\left(\frac{i}{M}\gamma_p\right) \right\}. \quad (33)$$

Hereby, depending on the above cases, the OP of the primary network for CSS-IAF scheme can be expressed as

$$P_{\mathrm{out}}^{\mathrm{AF}}(R_p) = \begin{cases} P_1(R_p), & \text{if } \gamma_p < \frac{\zeta}{1-\zeta}, \\ P_2(R_p), & \text{if } \frac{\zeta}{1-\zeta} \le \gamma_p < \frac{\zeta}{1-\zeta} + \gamma_p', \\ P_3(R_p), & \text{if } \gamma_p \ge \frac{\zeta}{1-\zeta} + \gamma_p'. \end{cases} \quad (34)$$

2) CSS WITH IDF RELAYING (CSS-IDF)

Considering a target rate R_p, the OP of the primary network for CSS-IDF scheme can be expressed as

$$P_{\mathrm{out}}^{\mathrm{DF}}(R_p) = \Pr\left[\gamma_{pq}^{\mathrm{DL}} < \gamma_p', \gamma_{ps}^{\mathrm{DL}} < \gamma_p\right] + \Pr\left[\gamma_{pq}^{\mathrm{DL}} < \gamma_p', \gamma_{ps}^{\mathrm{DL}} \ge \gamma_p, \gamma_{pq}^{\mathrm{DL}} + \gamma_{sq}^{\mathrm{DF}} < \gamma_p\right], \quad (35)$$

which can be further written as

$$P_{\mathrm{out}}^{\mathrm{DF}}(R_p) = \underbrace{F_{\gamma_{pq}^{\mathrm{DL}}}\left(\gamma_p'\right)F_{\gamma_{ps}^{\mathrm{DL}}}(\gamma_p)}_{I_3} + \underbrace{\bar{F}_{\gamma_{ps}^{\mathrm{DL}}}(\gamma_p)\Pr\left[\gamma_{pq}^{\mathrm{DL}} < \gamma_p', \gamma_{pq}^{\mathrm{DL}} + \gamma_{sq}^{\mathrm{DF}} < \gamma_p\right]}_{I_4}, \quad (36)$$

where $\bar{F}_{\gamma_{ps}^{\mathrm{DL}}}(\cdot) = 1 - F_{\gamma_{ps}^{\mathrm{DL}}}(\cdot)$ represents the complementary CDF. Hereby, to solve (36), it requires the assessment of the probability terms I_3 and I_4. To evaluate I_3, it further requires the CDFs $F_{\gamma_{pq}^{\mathrm{DL}}}(\gamma_p')$ and $F_{\gamma_{ps}^{\mathrm{DL}}}(\gamma_p)$, which can be deduced while accompanied by the steps as in Section III-A. However, I_4 can be computed in a similar fashion to (25), and is obtained as

$$I_4 \approx \Pr\left[\gamma_{pq}^{\mathrm{DL}} < \min\left(\gamma_p - \gamma_{sq}^{\mathrm{DF}}, \gamma_p'\right)\right]\bar{F}_{\gamma_{ps}^{\mathrm{DL}}}(\gamma_p) = \left[F_{\gamma_{pq}^{\mathrm{DL}}}\left(\gamma_p'\right)F_{\gamma_{sq}^{\mathrm{DF}}}\left(\gamma_p - \gamma_p'\right) + \sum_{i=0}^{M-1} \left\{ F_{\gamma_{pq}^{\mathrm{DL}}}\left(\frac{i+1}{M}\gamma_p\right) - F_{\gamma_{pq}^{\mathrm{DL}}}\left(\frac{i}{M}\gamma_p\right) \right\} F_{\gamma_{sq}^{\mathrm{DF}}}\left(\frac{M-i}{M}\gamma_p\right)\right]\bar{F}_{\gamma_{ps}^{\mathrm{DL}}}(\gamma_p). \quad (37)$$

To simplify (37), we need to find the CDF $F_{\gamma_{sq}^{\mathrm{DF}}}(\gamma_p - \gamma_p')$, which can be derived as in the following lemma.

Lemma 1: The CDF $F_{\gamma_{sq}^{\mathrm{DF}}}(x)$ under Nakagami-m fading can be deduced as

$$F_{\gamma_{sq}^{\mathrm{DF}}}(x) = \begin{cases} 1, & \text{if } x \ge \frac{\zeta}{1-\zeta}, \\ \phi_2(x), & \text{if } x < \frac{\zeta}{1-\zeta}, \end{cases} \quad (38)$$

where $\phi_2(x)$ is given as

$$\phi_2(x) = 1 - \sum_{k=0}^{m_{ps}-1} \frac{2}{k!}\left(\frac{T_0 x}{\theta_x}\right)^k \left(\frac{m_{sq}}{\Omega_{sq}}\right)^{m_{sq}} \frac{1}{\Gamma(m_{sq})} \times \left(\frac{T_0 x \Omega_{sq}}{\theta_x m_{sq}}\right)^{\frac{m_{sq}-k}{2}} \mathcal{K}_{m_{sq}-k}\left(2\sqrt{\frac{T_0 x m_{sq}}{\theta_x \Omega_{sq}}}\right). \quad (39)$$

Proof: Following the analogous steps as used in deriving (27) in Appendix A with (12), one can assess the result in (38). ■

By substituting the CDFs $F_{\gamma_{sq}^{\mathrm{DF}}}(x)$, $F_{\gamma_{pq}^{\mathrm{DL}}}(x)$, and $\bar{F}_{\gamma_{ps}^{\mathrm{DL}}}(x)$ into (37), I_4 can be obtained. Finally, after using the expressions for I_3 and I_4 into (36), and applying the conditions on

threshold γ_p with the help of (38), $P_{\text{out}}^{\text{DF}}(R_p)$ can be expressed for the following cases:

- When $\gamma_p < \frac{\zeta}{1-\zeta}$,

$$\begin{aligned} P_{\text{out}}^{\text{DF}}(R_p) &\triangleq P_4(R_p) \\ &= \Bigg[F_{\gamma_{pq}^{\text{DL}}}\left(\gamma_p'\right)F_{\gamma_{sq}^{\text{DF}}}\left(\gamma_p-\gamma_p'\right) \\ &\quad + \sum_{i=0}^{M-1}\left\{F_{\gamma_{pq}^{\text{DL}}}\left(\frac{i+1}{M}\gamma_p\right) - F_{\gamma_{pq}^{\text{DL}}}\left(\frac{i}{M}\gamma_p\right)\right\} \\ &\quad \times F_{\gamma_{sq}^{\text{DF}}}\left(\frac{M-i}{M}\gamma_p\right)\Bigg]\bar{F}_{\gamma_{ps}^{\text{DL}}}(\gamma_p) \\ &\quad + F_{\gamma_{pq}^{\text{DL}}}\left(\gamma_p'\right)F_{\gamma_{ps}^{\text{DL}}}(\gamma_p). \end{aligned} \tag{40}$$

- When $\frac{\zeta}{1-\zeta} \le \gamma_p < \frac{\zeta}{1-\zeta} + \gamma_p'$,

$$\begin{aligned} P_{\text{out}}^{\text{DF}}(R_p) &\triangleq P_5(R_p) \\ &= \Bigg[F_{\gamma_{pq}^{\text{DL}}}\left(\gamma_p'\right)F_{\gamma_{sq}^{\text{DF}}}\left(\gamma_p-\gamma_p'\right) \\ &\quad + \sum_{i=0}^{M-1}\left\{F_{\gamma_{pq}^{\text{DL}}}\left(\frac{i+1}{M}\gamma_p\right) - F_{\gamma_{pq}^{\text{DL}}}\left(\frac{i}{M}\gamma_p\right)\right\}\Bigg] \\ &\quad \times \bar{F}_{\gamma_{ps}^{\text{DL}}}(\gamma_p) + F_{\gamma_{pq}^{\text{DL}}}\left(\gamma_p'\right)F_{\gamma_{ps}^{\text{DL}}}(\gamma_p). \end{aligned} \tag{41}$$

- When $\gamma_p \ge \frac{\zeta}{1-\zeta} + \gamma_p'$,

$$\begin{aligned} P_{\text{out}}^{\text{DF}}(R_p) &\triangleq P_6(R_p) \\ &= \Bigg[F_{\gamma_{pq}^{\text{DL}}}\left(\gamma_p'\right) \\ &\quad + \sum_{i=0}^{M-1}\left\{F_{\gamma_{pq}^{\text{DL}}}\left(\frac{i+1}{M}\gamma_p\right) - F_{\gamma_{pq}^{\text{DL}}}\left(\frac{i}{M}\gamma_p\right)\right\}\Bigg] \\ &\quad \times \bar{F}_{\gamma_{ps}^{\text{DL}}}(\gamma_p) + F_{\gamma_{pq}^{\text{DL}}}\left(\gamma_p'\right)F_{\gamma_{ps}^{\text{DL}}}(\gamma_p). \end{aligned} \tag{42}$$

Thus, depending on the above cases, the OP of the primary network for the CSS-IDF scheme can be expressed as

$$P_{\text{out}}^{\text{DF}}(R_p) = \begin{cases} P_4(R_p), & \text{if } \gamma_p < \frac{\zeta}{1-\zeta}, \\ P_5(R_p), & \text{if } \frac{\zeta}{1-\zeta} \le \gamma_p < \frac{\zeta}{1-\zeta} + \gamma_p', \\ P_6(R_p), & \text{if } \gamma_p \ge \frac{\zeta}{1-\zeta} + \gamma_p'. \end{cases} \tag{43}$$

Remark 1: Referring to (34) and (43), it can be observed that the proposed CSS-IAF and CSS-IDF schemes are effective, when $\gamma_p < \frac{\zeta}{1-\zeta} + \gamma_p'$. Once $\gamma_p \ge \frac{\zeta}{1-\zeta} + \gamma_p'$, the RCC effect occurs, and hereby, the performance of the primary network solely depends on the DLT scheme. On the contrary, for the FR-based AF and DF relaying schemes, this RCC effect occurs once $\gamma_p \ge \frac{\zeta}{1-\zeta}$. Hence, the proposed IR-based schemes can support relatively higher data rate than the FR-based schemes till the occurrence of RCC effect. This implication is illustrated later in the Results and Discussion section.

C. NOMA-BASED POWER ALLOCATION PARAMETER

In order to accomplish the QoS criterion for the primary network, the NOMA power allocation strategy at relay node S must be developed. Herein, we choose the effective value of the NOMA-based power allocation parameter ζ such that the OP of primary network for CSS scheme lies below or equal to that for DLT scheme. From (34) and (43), referring the condition $\gamma_p < \frac{\zeta}{1-\zeta} + \gamma_p'$, the permissible range of ζ under the CSS-IAF and CSS-IDF schemes for a given threshold γ_p can be calculated as

$$\frac{\gamma_p - \gamma_p'}{1 + \gamma_p - \gamma_p'} < \zeta < 1. \tag{44}$$

Consequently, the effective value of ζ can be evaluated for a given target rate R_p under the CSS-IAF and CSS-IDF schemes based on the respective conditions

$$P_{\text{out}}^{\text{AF}}(R_p) \le P_{\text{out}}^{\text{DL}}(R_p) \tag{45}$$

and

$$P_{\text{out}}^{\text{DF}}(R_p) \le P_{\text{out}}^{\text{DL}}(R_p). \tag{46}$$

Note that a lower value of ζ can allocate more power to the secondary communication, resulting in better CSS possibilities. Since the PR is a high-priority NOMA recipient, a higher value of ζ is assigned to the PR.

IV. OUTAGE PERFORMANCE OF SECONDARY NETWORK

This section provides the OP expression for the secondary network under both the CSS-IAF and CSS-IDF schemes while considering the two cases of SIC, i.e., ipSIC and pSIC.

A. CSS-IAF SCHEME

Considering a target rate R_s, the OP of the secondary network for the CSS-IAF scheme can be expressed as

$$\begin{aligned} P_{\text{out}}^{\text{AF}}(R_s) &= \Pr\left[\gamma_{pq}^{\text{DL}} \ge \gamma_p', \gamma_{sr}^{\text{noc}} < \gamma_s\right] \\ &\quad + \Pr\left[\gamma_{pq}^{\text{DL}} < \gamma_p', \gamma_{psr}^{\text{AF}} < \gamma_s\right], \end{aligned} \tag{47}$$

where $\gamma_s = 2^{\frac{2R_s}{1-\alpha}} - 1$. Further, $P_{\text{out}}^{\text{AF}}(R_s)$ in (47) can be expressed as

$$P_{\text{out}}^{\text{AF}}(R_s) = \bar{F}_{\gamma_{pq}^{\text{DL}}}\left(\gamma_p'\right)F_{\gamma_{sr}^{\text{noc}}}(\gamma_s) + F_{\gamma_{pq}^{\text{DL}}}\left(\gamma_p'\right)F_{\gamma_{psr}^{\text{AF}}}(\gamma_s). \tag{48}$$

As discussed, we evaluate the $F_{\gamma_{psr}^{\text{AF}}}(\gamma_s)$ for the ipSIC and pSIC cases as given in the subsequent subsections.

1) IPSIC

Hereby, $F_{\gamma_{psr}^{\text{AF}}}(\gamma_s)$ in (48) can be obtained for the case of ipSIC as given in the following theorem.

Theorem 2: The CDF $F_{\gamma_{psr}^{\text{AF}}}(\gamma_s)$ for the case of ipSIC in CSS-IAFscheme for EH-OCNOMA system under

Nakagami-m fading can be given by

$$F_{\gamma_{psr}^{\mathrm{AF}}}(\gamma_s) = \Psi_1(\gamma_s) - \Psi_2(\gamma_s), \tag{49}$$

where $\Psi_1(\gamma_s)$ and $\Psi_2(\gamma_s)$ are given as

$$\Psi_1(\gamma_s) = \sum_{k=0}^{m_{sr}-1} \frac{(T_2\zeta)^k}{k!} \frac{1}{\Gamma(m_R)} \left(\frac{m_R}{\Omega_R}\right)^{m_R} (k+m_R-1)! \times \left(T_2\zeta + \frac{m_R}{\Omega_R}\right)^{-(k+m_R)}, \tag{50}$$

$$\begin{aligned}\Psi_2(\gamma_s) = {} & \sum_{k=0}^{m_{ps}-1} \sum_{j=0}^{k} \sum_{m=0}^{j+m_{sr}-1} \sum_{v=0}^{j+m_R+m_{sr}-2-m} \frac{2(T_0\gamma_s)^k}{k!} \\ & \times \frac{1}{\Gamma(m_{sr})} \left(\frac{m_{sr}}{\Omega_{sr}}\right)^{m_{sr}} \frac{1}{\Gamma(m_R)} \left(\frac{m_R}{\Omega_R}\right)^{m_R} \binom{k}{j} (\zeta\beta)^j \\ & \times \binom{j+m_{sr}-1}{m} (\zeta\gamma_s)^{j+m_{sr}-1-m} e^{\left(\frac{T_2T_1}{\zeta\beta\gamma_s} - \frac{T_0\gamma_s\zeta\beta}{T_1} + T_3\right)} \\ & \times \binom{j+m_{sr}+m_R-2-m}{v} \left(\frac{T_1}{\zeta^2\beta\gamma_s}\right)^{j+m_R+m_{sr}-1-m} \\ & \times \left(\frac{T_0\gamma_s T_1\Omega_{sr}}{m_{sr}}\right)^{\frac{m+1-k}{2}} (-1)^{j+m_R+m_{sr}-2-m-v} \\ & \times \left(\frac{1}{T_1}\right)^{j+m_{sr}} \int_1^{\infty} \theta^{\frac{m+2v+1-k}{2}} e^{-\left(\frac{T_2T_1\theta}{\zeta^2\beta\gamma_s} + T_3\theta\right)} \\ & \times \mathcal{K}_{m-k+1}\left(2\sqrt{\frac{m_{sr}T_0\gamma_s\theta}{\Omega_{sr}T_1}}\right) d\theta, \end{aligned} \tag{51}$$

with $T_1 = (1-\zeta)$, $T_2 = \frac{m_{sr}\gamma_s}{\Omega_{sr}T_1}$, and $T_3 = \frac{m_RT_1}{\Omega_R\zeta^2\beta\gamma_s}$.

Proof: See Appendix B. ■

Although the expression in (51) is presented in a one-integral form, it can be efficiently computed using symbolic software like Mathematica or Maple and consumes much less time than the computer simulation approach.

2) PSIC

For the pSIC case, the $F_{\gamma_{psr}^{\mathrm{AF}}}(\gamma_s)$ can be evaluated as in the following lemma.

Lemma 2: The CDF $F_{\gamma_{psr}^{\mathrm{AF}}}(\gamma_s)$ for the case of pSIC under Nakagami-m fading can be given by

$$\begin{aligned} F_{\gamma_{psr}^{\mathrm{AF}}}(\gamma_s) = 1 - 2 & \sum_{k=0}^{m_{ps}-1} \sum_{j=0}^{k} \left(\frac{T_0\gamma_s}{T_1}\right)^k \frac{1}{k!} e^{\frac{-T_0\gamma_s\zeta\beta}{T_1}} \binom{k}{j} \\ & \times (\zeta\beta)^j \frac{1}{\Gamma(m_{sr})} \left(\frac{m_{sr}}{\Omega_{sr}}\right)^{m_{sr}} \left(\frac{T_0\gamma_s\Omega_{sr}}{T_1m_{sr}}\right)^{\frac{j-k+m_{sr}}{2}} \\ & \times \mathcal{K}_{j-k+m_{sr}}\left(2\sqrt{\frac{T_0\gamma_sm_{sr}}{T_1\Omega_{sr}}}\right). \end{aligned} \tag{52}$$

Proof: By adopting the similar steps as followed for (49) in Appendix B, one can get the result in (52). ■

Next, $F_{\gamma_{sr}^{\mathrm{noc}}}(\gamma_s)$ can be obtained using (18) with the help of following lemma as follows:

Lemma 3: The CDF $F_{\gamma_{sr}^{\mathrm{noc}}}(\gamma_s)$ for the no cooperation case under Nakagami-m fading can be given by

$$\begin{aligned} F_{\gamma_{sr}^{\mathrm{noc}}}(\gamma_s) = 1 - 2 & \sum_{k=0}^{m_{ps}-1} \frac{(T_0\gamma_s)^k}{k!} \frac{1}{\Gamma(m_{sr})} \left(\frac{m_{sr}}{\Omega_{sr}}\right)^{m_{sr}} \\ & \times \left(\frac{T_0\gamma_s\Omega_{sr}}{m_{sr}}\right)^{\frac{m_{sr}-k}{2}} \mathcal{K}_{m_{sr}-k}\left(2\sqrt{\frac{T_0\gamma_sm_{sr}}{\Omega_{sr}}}\right). \end{aligned} \tag{53}$$

Proof: See Appendix C. ■

Hereby, the desired OP for the cases of ipSIC and pSIC can be evaluated by substituting the involved CDF expressions in (48).

B. CSS-IDF SCHEME

Considering a target rate R_s, the OP of the secondary network for the CSS-IDF scheme can be expressed as

$$\begin{aligned} P_{\mathrm{out}}^{\mathrm{DF}}(R_s) = {} & \Pr\left[\gamma_{pq}^{\mathrm{DL}} \geq \gamma_p', \gamma_{sr}^{\mathrm{noc}} < \gamma_s\right] \\ & + \Pr\left[\gamma_{pq}^{\mathrm{DL}} < \gamma_p', \gamma_{ps}^{\mathrm{DL}} < \gamma_p, \gamma_{sr}^{\mathrm{noc}} < \gamma_s\right] \\ & + \Pr\left[\gamma_{pq}^{\mathrm{DL}} < \gamma_p', \gamma_{ps}^{\mathrm{DL}} \geq \gamma_p, \gamma_{sr}^{\mathrm{DF}} < \gamma_s\right], \end{aligned} \tag{54}$$

which can be further expressed as

$$\begin{aligned} P_{\mathrm{out}}^{\mathrm{DF}}(R_s) = {} & \bar{F}_{\gamma_{pq}^{\mathrm{DL}}}\left(\gamma_p'\right) F_{\gamma_{sr}^{\mathrm{noc}}}(\gamma_s) \\ & + F_{\gamma_{pq}^{\mathrm{DL}}}\left(\gamma_p'\right) \underbrace{\Pr\left[\gamma_{ps}^{\mathrm{DL}} < \gamma_p, \ \gamma_{sr}^{\mathrm{noc}} < \gamma_s\right]}_{P_1} \\ & + F_{\gamma_{pq}^{\mathrm{DL}}}\left(\gamma_p'\right) \underbrace{\Pr\left[\gamma_{ps}^{\mathrm{DL}} \geq \gamma_p, \gamma_{sr}^{\mathrm{DF}} < \gamma_s\right]}_{P_2}. \end{aligned} \tag{55}$$

As such, (55) requires the evaluation of the two probability terms P_1 and P_2. Hereby, we first evaluate the probability term P_1 as

$$P_1 = \Pr\left[\gamma_{ps}^{\mathrm{DL}} < \gamma_p, \ \gamma_{sr}^{\mathrm{noc}} < \gamma_s\right], \tag{56}$$

which can be re-expressed using (18) as

$$\begin{aligned} P_1 &= \Pr\left[\gamma_{ps}^{\mathrm{DL}} < \gamma_p, \ \beta\gamma_{ps}|h_{sr}|^2 < \gamma_s\right] \\ &= \Pr\left[\gamma_{ps}^{\mathrm{DL}} < \min\left(\gamma_p, \ \frac{\gamma_s}{\beta|h_{sr}|^2}\right)\right] \\ &= \underbrace{\Pr\left[\gamma_{ps}^{\mathrm{DL}} < \gamma_p, \ \gamma_p < \frac{\gamma_s}{\beta|h_{sr}|^2}\right]}_{P_{11}} \\ &\quad + \underbrace{\Pr\left[\gamma_{ps}^{\mathrm{DL}} < \frac{\gamma_s}{\beta|h_{sr}|^2}, \ \gamma_p \geq \frac{\gamma_s}{\beta|h_{sr}|^2}\right]}_{P_{12}}, \end{aligned} \tag{57}$$

where P_{11} can be given as

$$P_{11} = F_{\gamma_{ps}^{\mathrm{DL}}}(\gamma_p) F_{|h_{sr}|^2}\left(\frac{\gamma_s}{\beta\gamma_p}\right). \tag{58}$$

To evaluate P_{11}, we require the CDFs $F_{\gamma_{ps}^{\mathrm{DL}}}(\gamma_p)$ and $F_{|h_{sr}|^2}(\frac{\gamma_s}{\beta\gamma_p})$, which can be obtained readily using (20). Now, the next probability term P_{12} in (57) can be computed through the following lemma.

Lemma 4: The probability term P_{12} in (57) can be expressed under Nakagami-m fading as

$$P_{12} = \sum_{k=0}^{m_{sr}-1} \frac{1}{k!}\left(\left(\frac{T_2T_1}{\beta\gamma_p}\right)^k e^{\left(-\frac{T_2T_1}{\beta\gamma_p}\right)} - 2\left(\frac{T_1T_2}{\eta_p}\right)^k \left(\frac{m_{ps}}{\Omega_{ps}}\right)^{m_{ps}} \times \frac{1}{\Gamma(m_{ps})}\left(\frac{T_1T_2\Omega_{ps}}{\eta_p m_{ps}}\right)^{\frac{m_{ps}-k}{2}} \times \mathcal{K}_{m_{ps}-k}\left(2\sqrt{\frac{T_1T_2m_{ps}}{\eta_p\Omega_{ps}}}\right)\right). \quad (59)$$

Proof: See Appendix D. ∎

Next, we evaluate the other probability term P_2 in (55) for the ipSIC and pSIC cases in the sequel.

1) IPSIC

For this case, we proceed with the analysis using the following lemma.

Lemma 5: The probability term P_2 in (55) for the ipSIC case under Nakagami-m fading can be given as

$$P_2 = \bar{F}_{\gamma_{ps}^{\mathrm{DL}}}(\gamma_p)P_{21} - P_{22}, \quad (60)$$

where P_{21} and P_{22} are given by

$$P_{21} = \sum_{k=0}^{m_{sr}-1} \frac{(T_2\zeta)^k}{k!}\frac{1}{\Gamma(m_R)}\left(\frac{m_R}{\Omega_R}\right)^{m_R}(k+m_R-1)! \times \left(T_2\zeta + \frac{m_R}{\Omega_R}\right)^{-(k+m_R)},$$

$$P_{22} = \sum_{k=0}^{m_{ps}-1}\sum_{j=0}^{m_{sr}-1} \frac{2(T_0\gamma_s)^k}{k!}\frac{1}{\Gamma(m_{sr})}\left(\frac{m_{sr}}{\Omega_{sr}T_1}\right)^{m_{sr}} \times \binom{m_{sr}-1}{j}(\zeta\gamma_s)^j \frac{1}{\Gamma(m_R)}\left(\frac{m_R}{\Omega_R}\right)^{m_R} \times \left(\frac{T_0\gamma_sT_1\Omega_{sr}}{m_{sr}}\right)^{\frac{m_{sr}-j-k}{2}} \mathcal{K}_{m_{sr}-j-k}\left(2\sqrt{\frac{m_{sr}T_0\gamma_s}{\Omega_{sr}T_1}}\right) \times (m_R+j-1)!\left(T_2\zeta + \frac{m_R}{\Omega_R}\right)^{-(m_R+j)}. \quad (61)$$

Proof: By adopting the similar procedure used for the derivation of (59) in Appendix D, one can get the result in (60). ∎

2) PSIC

For the pSIC case, the analysis can be conducted further with the aid of following lemma.

Lemma 6: For the pSIC case, the probability term P_2 in (55) can be computed under Nakagami-m fading as

$$P_2 = P_{23} - F_{\gamma_{ps}^{\mathrm{DL}}}(\gamma_p), \quad (62)$$

where P_{23} is given by

$$P_{23} = 1 - 2\sum_{k=0}^{m_{ps}-1}\left(\frac{T_0\gamma_s}{T_1}\right)^k \frac{1}{\Gamma(m_{sr})}\left(\frac{m_{sr}}{\Omega_{sr}}\right)^{m_{sr}}\frac{1}{k!} \times \left(\frac{T_0\gamma_s\Omega_{sr}}{T_1m_{sr}}\right)^{\frac{m_{sr}-k}{2}} \mathcal{K}_{m_{sr}-k}\left(2\sqrt{\frac{T_0\gamma_sm_{sr}}{T_1\Omega_{sr}}}\right). \quad (63)$$

Proof: By following the same line of derivation used to obtain (59) in Appendix D, one can get the result in (62). ∎

Thus, the required OP for the cases of ipSIC and pSIC can be evaluated by inserting the associated CDF and above-mentioned probability expressions in (55).

Remark 2: Under the proposed CSS schemes, ST can apply NOMA only when the target rate of the primary network is not satisfied. Otherwise, secondary communication takes place separately in conjunction with primary communication. Therefore, the performance of the secondary network is greatly influenced by the parameters of the primary network. As such, the impact of ipSIC/pSIC may become insignificant depending upon m_{pq} and γ_p of primary communication network.

V. OVERALL EH-OCNOMA SYSTEM PERFORMANCE

This section investigates the throughput and energy efficiency measures for the considered EH-OCNOMA system based on the outcomes in previous sections.

A. SYSTEM THROUGHPUT

The system throughput is a crucial performance metric for evaluating the spectrum utilization of the considered EH-OCNOMA. It essentially signifies the mean spectral efficiency for cooperative communication based wireless networks [54], [55]. In this paper, it is defined as the sum of individual target rates for both the primary and secondary communications that can be accomplished successfully over the Nakagami-m fading channels. Relying on the results derived in Sections III and IV, we obtain here the system throughput for the respective CSS-IAF and CSS-IDF schemes as

$$\mathcal{S}_T^{\mathrm{AF}} = \frac{(1-\alpha)}{2}\left[\left(1 - P_{\mathrm{out}}^{\mathrm{AF}}(R_p)\right)R_p + \left(1 - P_{\mathrm{out}}^{\mathrm{AF}}(R_s)\right)R_s\right] \quad (64)$$

and

$$\mathcal{S}_T^{\mathrm{DF}} = \frac{(1-\alpha)}{2}\left[\left(1 - P_{\mathrm{out}}^{\mathrm{DF}}(R_p)\right)R_p + \left(1 - P_{\mathrm{out}}^{\mathrm{DF}}(R_s)\right)R_s\right]. \quad (65)$$

It can be observed that the maximum achievable system throughput is $\Re(1-\alpha)$ with setting $R_p = R_s = \Re$ for both the proposed schemes, which could be attained with pSIC conditions at a high SNR region, as the OP approaches zero.

B. ENERGY EFFICIENCY

Based on the throughput expressions in (64) and (65), one can quantify the energy efficiency of the considered EH-OCNOMA system under the CSS-IAF and CSS-IDF schemes. As a result of such analysis, an EH-OCNOMA system with an extended network lifespan can be designed. Fundamentally, the system energy efficiency refers to the ratio between the amount of data delivered and the amount of energy consumed [54], [56]. The system throughput represents the total amount of data delivered as given in (64) and (65) for the CSS-IAF and CSS-IDF schemes, respectively. The energy consumed by the PT in the EH phase (of duration αT) and in the first IT phase (of duration $(1-\alpha)T/2$) accounts for the overall energy consumed in the TS-based EH approach for the considered system. It should be emphasized that the energy consumed in the second IT phase is the energy harvested by node S in the EH phase, and thus, does not contribute to the overall energy consumed in the system. Hence, the energy efficiency for the proposed EH-OCNOMA system under the CSS-IAF and CSS-IDF schemes can be expressed as

$$\Xi^{\mathrm{AF}} = \frac{\mathcal{S}_T^{\mathrm{AF}}}{P_p\left[\alpha + \frac{(1-\alpha)}{2}\right]} \tag{66}$$

and

$$\Xi^{\mathrm{DF}} = \frac{\mathcal{S}_T^{\mathrm{DF}}}{P_p\left[\alpha + \frac{(1-\alpha)}{2}\right]}, \tag{67}$$

where $\mathcal{S}_T^{\mathrm{AF}}$ and $\mathcal{S}_T^{\mathrm{DF}}$ in bps/Hz are given in (64) and (65), respectively.

Remark 3: We can observe that the harvested energy at the ST increases with increase in TS parameter α, where $\alpha \in (0, 1)$ refers to the fraction of transmission block time T for EH and rest $(1-\alpha)$ for IT. On the contrary, an increase in α also brings a decrease in IT time. Thereby, with the initial increase in α, the system throughput improves as a result of the more harvested energy at the ST. However, with a further increase in α, the degradation in system throughput results due to the decreased IT time.

VI. RESULTS AND DISCUSSION

This section carries out the numerical findings to validate our analytical expressions derived in the previous sections and endorses the results further through Monte-Carlo simulations, while examining the impact of critical measures on the system performance. For the proposed EH-OCNOMA system, we plot the curves based on the mathematical analysis for the two CSS schemes build on the IR protocol using AF and DF strategies, viz., CSS-IAF and CSS-IDF. Further, we plot the curves for the FR-based AF and DF relaying schemes through simulations to compare their performance with the proposed schemes. It is demonstrated from the various figures that the proposed schemes improve the overall performance of considered EH-OCNOMA in terms of the OP, system throughput, and energy efficiency. Moreover, DF relaying outperforms the AF relaying for both IR and FR based schemes. Unless otherwise stated, we set the following parameters: $m_{pq} = 1$, $m_{ps} = 2$, $m_{sq} = m_{sr} = m_R = 3$ as fading severity parameters, $\Omega_{pq} = \Omega_{ps} = \Omega_{sq} = 1$, $\Omega_{sr} = 16$ as the average power[6] of the multipath components, $\Omega_R = 0.01$ as the mean value of the IS channel power gain, $\alpha = 0.18$ as the TS parameter, $\Theta = 0.7$ as the energy conversion efficiency, η_p as the SNR, $N_o = 1$, and block duration $T = 1$ sec. We also set $M = 50$ in Section III-B to significantly reduce the approximation error [53].

In Fig. 4, we plot the OP versus SNR curves for the primary network under the AF and DF relaying to show the impact of various values of target rates (R_p). Herein, we set $R_p = 0.5, 1.0$ bps/Hz. Based on the values of R_p and α, we decide the appropriate value of ζ for the CSS-IAF and CSS-IDF schemes according to Section III-C. It can be observed that the proposed schemes outperform the FR-based schemes over the entire SNR regime, and the performance of the DF relaying strategy is slightly better than that of the AF relaying one. Further, the OP performance for the baseline DLT scheme and the OMA scheme is also depicted for comparison purposes. From the plot, one can observe that the proposed CSS schemes considerably outperform the DLT scheme in the medium-to-high SNR regime. This is because of the additional diversity gain obtained through the proposed CSS schemes. The CSS schemes with NOMA surpass the OMA scheme for the high data rate requirements. Since the OMA scheme requires three time slots to execute its operation [22], the target SINR threshold (for a fixed value of target rate) relatively increases for the OMA scheme which degrades its performance. However, for the low data rate requirements, the OMA scheme can provide better performance compared to NOMA in the low SNR region. Moreover, it is evident that as the target rate increases from $R_p = 0.5$ to 1.0 bps/Hz, the outage performance of the primary network degrades.

Fig. 5 depicts the OP versus threshold γ_p for the primary network to show the superiority of proposed IR-based schemes over the FR-based schemes. For this, we set the SNR as $\eta_p = 30$ dB. We further select the value of ζ based on fulfilling the QoS criteria as discussed in Section III-C. From the figure, one can observe that the OP degrades as the value of γ_p increases. When the threshold approaches $\gamma_p = \frac{\zeta}{1-\zeta} + \gamma_p'$ [refer to (34) and (43)] for both CSS-IAF and CSS-IDF schemes, the RCC effect occurs, and hereby, the performance of the proposed schemes follow the DLT scheme. On the contrary, for the FR-based schemes, this RCC effect takes place relatively at the lower value of threshold, i.e., $\gamma_p = \frac{\zeta}{1-\zeta}$. Hence, the proposed schemes can support

6. In the path loss environment, the average power of fading channel coefficients are presented as $\Omega_{ij} = d_{ij}^{-\nu}$ [57], where d_{ij} is the normalized distance between transmit node i and receive node j, and ν be the path loss exponent which is function of carrier frequency, environment, obstructions, etc. It typically ranges from 2 to 6 (at around 1 GHz) in the free-space loss to the dense urban environmental conditions, correspondingly. As such, in the RF-based EH system, the RF energy must be extracted at very low power density since the propagation energy drops off at the rate of $d_{ij}^{-\nu}$.

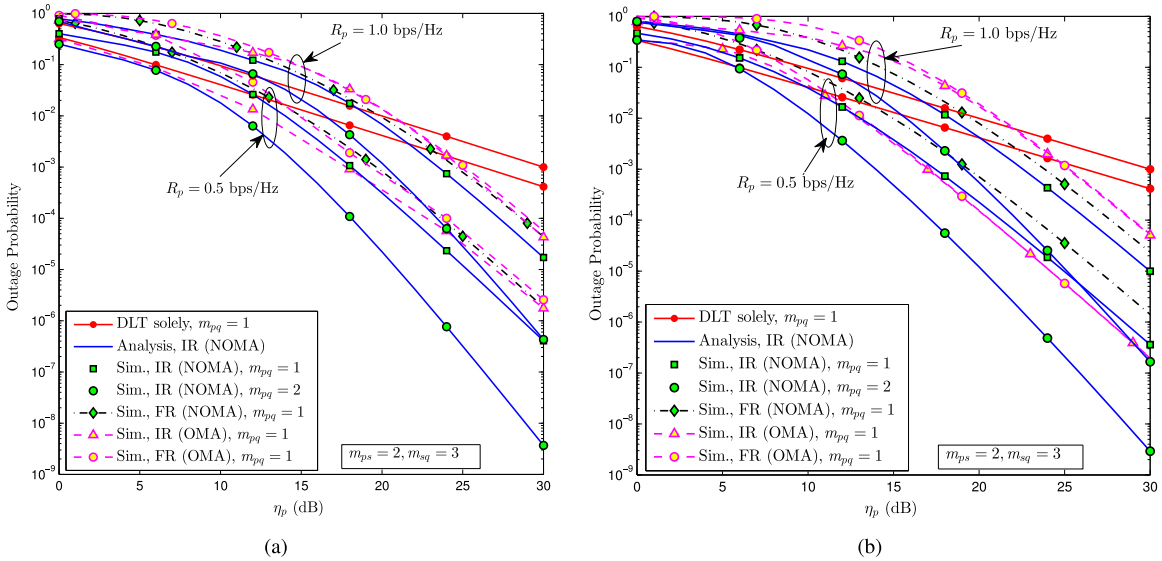

FIGURE 4. OP versus SNR plots for the primary network with different target rates (R_p) (a) AF (b) DF.

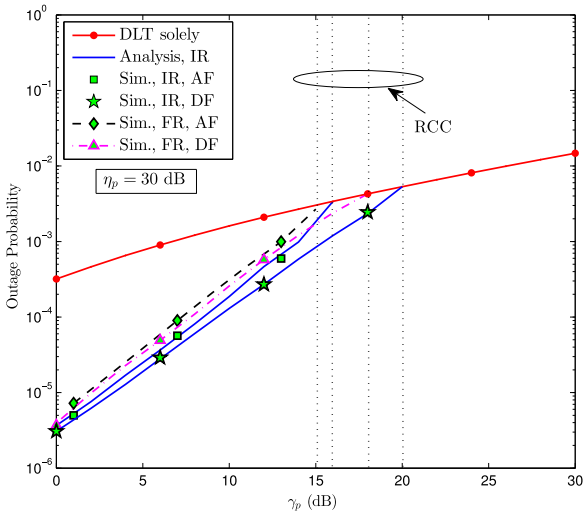

FIGURE 5. OP versus γ_p plots for the primary network.

comparatively higher data rates till the occurrence of RCC effect.

Fig. 6 illustrates the OP performance of the secondary network under the AF and DF relaying strategies using the derived analytical expressions in Section IV. For this, we particularly plot the curves for both ipSIC and pSIC cases while setting the values of target rates as $R_p = R_s = 1.0$ bps/Hz. Resorting to the values of target rates and α, we find the respective values of ζ for the CSS-IAF and CSS-IDF schemes. The performance gap between pSIC and ipSIC cases, which is more pronounced for AF than DF relaying, diminishes with the increase of $m_{pq} = 1, 2, 3$. This is because better primary channel condition helps the primary network to meet its target rate and thereby relaxes the requirement of NOMA-based cooperative relaying by the secondary network. We can also see that, under the case of pSIC, the CSS schemes with NOMA offer relatively better outage performance than the benchmark OMA scheme.

Fig. 7 shows the impact of ipSIC on the OP performance of secondary network by varying the values of Ω_R. For this, we set $R_p = R_s = 1.0$ bps/Hz. As can be seen from the figure, the OP performance improves with the decrease in the level of ipSIC ($\Omega_R = -3, -10, -20$ dB), especially when $\{m_{pq} = 1, m_{ps} = 2, m_{sr} = 3\}$. We can further see that when Ω_R decreases, the secondary network performance gets more improved under the CSS-IDF scheme as compared with the CSS-IAF scheme in the high SNR regime. This is because the performance of secondary network improves under CSS-IDF scheme when m_{ps} increases as it can help in decoding of primary signal at the ST node (relay). The impact of ipSIC/pSIC gets insignificant as the value of m_{pq} increases. This is attributed to the fact that NOMA based relaying at the ST node is employed only when the target rate of the primary network is not satisfied. Otherwise, ST utilizes all the harvested power for its own communication only.

Fig. 8 exhibits the system throughput versus SNR curves for two distinct values of target rates ($R_p = R_s = 0.5, 1.0$ bps/Hz). One can observe from the figure that the proposed IR-based schemes substantially improve the system throughput as compared to the FR-based schemes, specially in low-to-medium SNR regime. In the high SNR region, the system throughput saturates as the OP tends to zero. Thus, the maximum system throughput for both the FR- and IR-based schemes become the sum of individual target rates of the primary and secondary networks.

Fig. 9 shows the impact of the SNR on the energy efficiency of the proposed EH-OCNOMA system for two different values of target rates ($R_p = R_s = 0.5, 1.0$ bps/Hz)

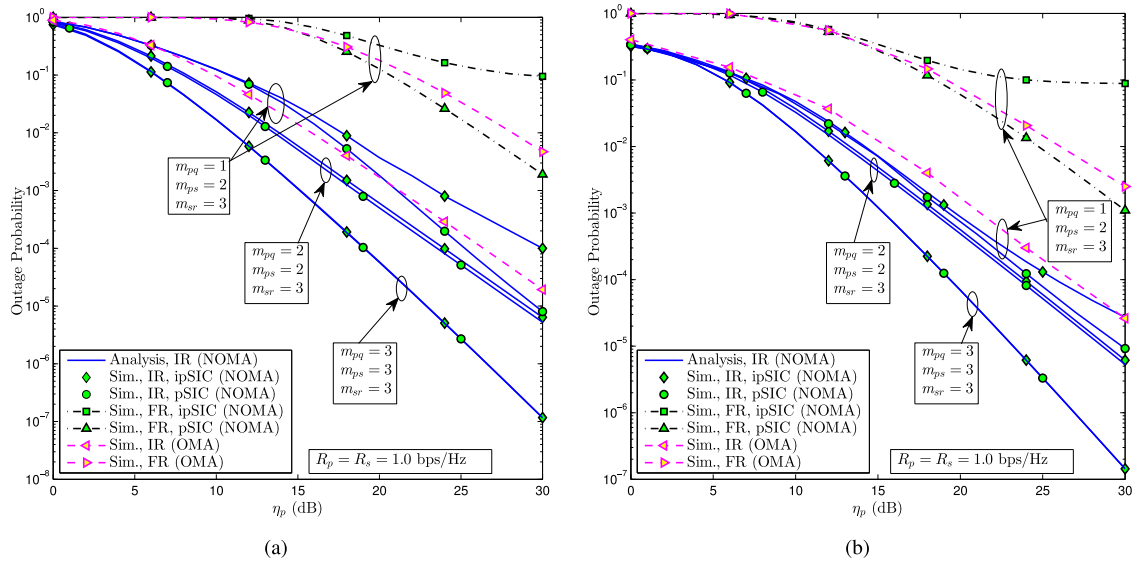

FIGURE 6. OP versus SNR plots for the secondary network (a) AF (b) DF.

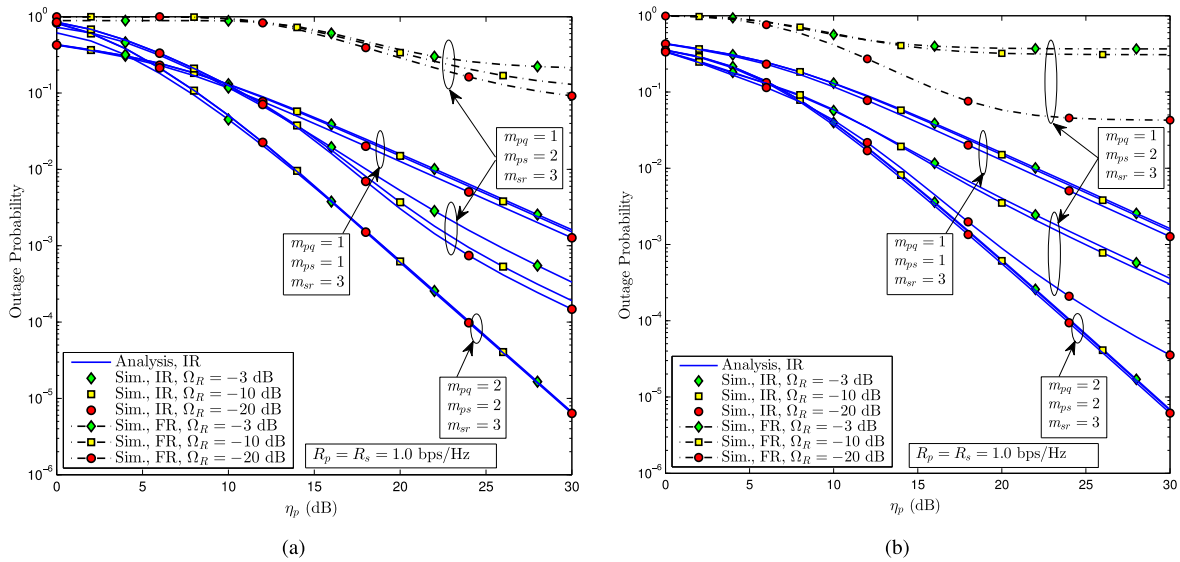

FIGURE 7. Impact of ipSIC on the OP performance of secondary network (a) AF (b) DF.

under the AF and DF relaying strategies. It can be observed from the curves that the energy efficiency is maximal at a certain value of the SNR for a particular target rate. By varying the target rate, the SNR value at which systems achieves maximum energy efficiency also varies. It is also worth noting that the system energy efficiency is lowest in the high SNR region, because the utilized power is much higher than the system throughput at higher SNR values. Further, it can be observed that the IR protocol is more energy efficient than the FR protocol.

Fig. 10 depicts the impacts of the TS parameter α and energy conversion factor Θ on the system throughput for a certain value of target rates ($R_p = R_s = 1.0$ bps/Hz). From the curves, it can be visualized that when α increases, the system throughput initially increases up to some extent, and afterwards, it starts to decrease. Hereby, one can observe an effective value of α around 0.18. Such performance characteristic conforms that the harvested energy at the ST increases with an increase in α. However, an increase in α subsequently decreases the IT time. Thereby, with the initial increase in α, the system throughput improves as a result of more harvested energy at the ST. However, with a further increase in α, the degradation in system throughput results due to the decreased IT time. The effective value of α decreases for the CSS-IAF scheme as compared to the CSS-IDF scheme. On the other hand, when Θ increases, the throughput performance of the EH-OCNOMA system upgrades. It accords with the basic fact that the amount of energy harvested in

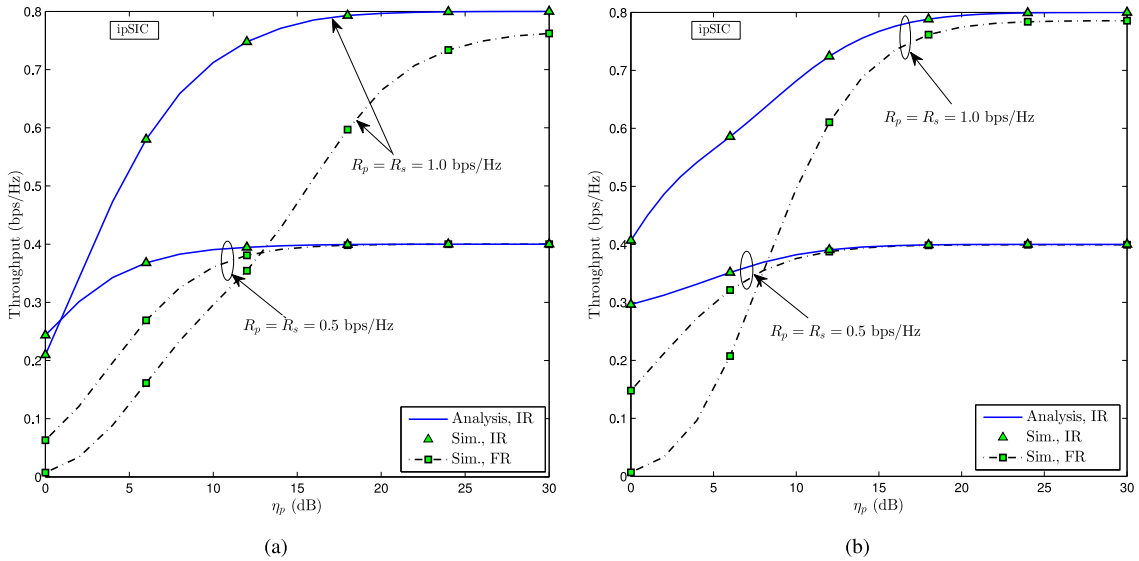

FIGURE 8. Throughput versus SNR plots for the EH-OCNOMA system (a) AF (b) DF.

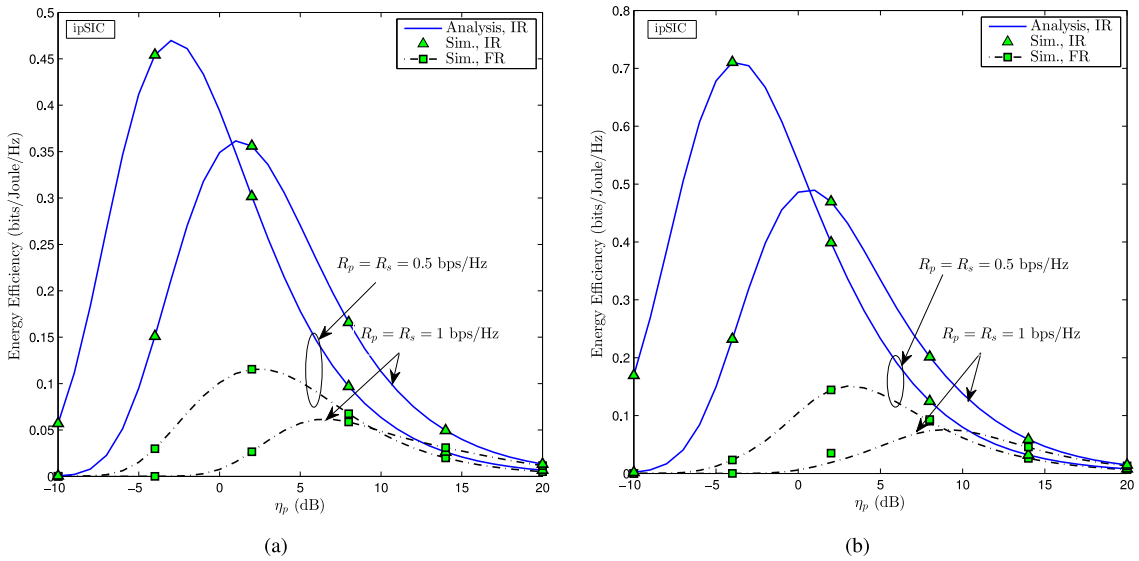

FIGURE 9. Energy efficiency versus SNR plots for the EH-OCNOMA system (a) AF (b) DF.

EH phase increases as the energy conversion factor Θ increases.

VII. CONCLUSION

In this paper, we investigated the performance of an EH-OCNOMA system over the Nakagami-*m* fading channel, wherein an energy-constrained ST node has been assumed to cooperate with the primary signal transmission while simultaneously transmitting its own information using the NOMA principle. For this, we proposed two CSS schemes based on IR protocol using the AF and DF relaying strategies, viz., CSS-IAF and CSS-IDF, and compared their performance with the conventional FR-based AF and DF relaying schemes, DLT scheme, and OMA scheme. The proposed schemes have significantly improved the performance of both primary and secondary networks over the baseline schemes, as the proposed schemes efficiently utilize the available spectrum resources to improve the system performance. Further, to get more insight, we examined the system throughput and energy efficiency for the considered EH-OCNOMA system. Above all, a comparison with FR-based schemes reveals that the proposed schemes can support relatively higher data rates till the occurrence of the RCC effect. Further, the CSS-IDF scheme illustrates comparatively better performance than its CSS-IAF counterpart. Additionally, the performance of secondary network is significantly improved for the CSS-IDF scheme.

For future work, it would be intriguing to execute the EH-OCNOMA system performance analysis while deploying the PT with multiple antennas and considering the spatial

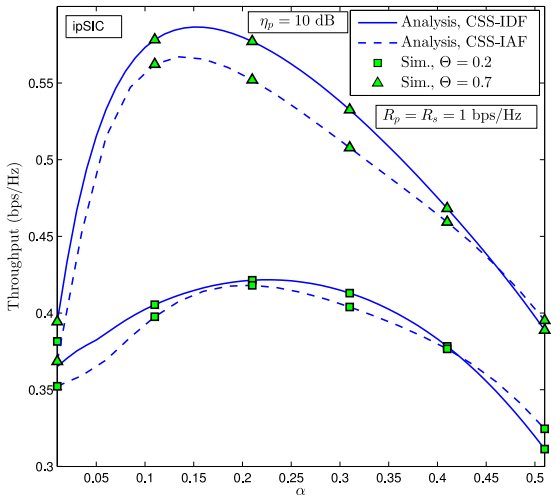

FIGURE 10. Throughput versus α plots for the EH-OCNOMA system.

correlation among the communication links. Further, considering various non-linear electronic devices in the energy harvester circuitry, one can study a non-linear EH model for OCNOMA system. Nevertheless, our presented results will serve as a benchmark of the EH-OCNOMA system performance and provide useful guidelines for the design of 5G and beyond wireless networks.

APPENDIX A

Referring to (7), the CDF $F_{\gamma_{psq}^{\mathrm{AF}}}(x) = \Pr[\gamma_{psq}^{\mathrm{AF}} < x]$ can be expressed as

$$F_{\gamma_{psq}^{\mathrm{AF}}}(x) = \Pr\left[\frac{\zeta\gamma_{ps}\beta|h_{sq}|^2}{(1-\zeta)\gamma_{ps}\beta|h_{sq}|^2 + \zeta\beta|h_{sq}|^2 + 1} < x\right] = \Pr\left[\gamma_{ps} < \frac{x(1+\zeta\beta|h_{sq}|^2)}{\theta_x\beta|h_{sq}|^2}\right], \tag{68}$$

which can be further evaluated as

$$F_{\gamma_{psq}^{\mathrm{AF}}}(x) = \int_0^\infty F_{\gamma_{ps}}\left(\frac{x(1+\zeta\beta y)}{\theta_x\beta y}\right) f_{|h_{sq}|^2}(y)dy. \tag{69}$$

With $\theta_x > 0$, on substituting the PDF $f_{|h_{sq}|^2}(\cdot)$ and the CDF $F_{\gamma_{ps}}(\cdot)$ using (19) and (20), respectively, and then solving by using the binomial expansion [43, eq. (1.111)], we get $F_{\gamma_{psq}^{\mathrm{AF}}}(x)$ as given in (27) with $\phi_1(x)$ as

$$\phi_1(x) = 1 - \sum_{k=0}^{m_{ps}-1}\sum_{j=0}^{k}\frac{1}{k!}\left(\frac{T_0 x}{\theta_x}\right)^k \mathrm{e}^{-\left(\frac{T_0 x\zeta\beta}{\theta_x}\right)}\left(\frac{m_{sq}}{\Omega_{sq}}\right)^{m_{sq}}\binom{k}{j} \times \frac{1}{\Gamma(m_{sq})}(\zeta\beta)^j\int_0^\infty y^{(m_{sq}+j-k)-1}\mathrm{e}^{-\frac{T_0 x}{\theta_x y}-\frac{m_{sq}}{\Omega_{sq}}y}. \tag{70}$$

Finally, by computing the involved integral using [43, eq. (3.471.9)], one can reach the desired result as provided in (28).

APPENDIX B

The CDF $F_{\gamma_{psr}^{\mathrm{AF}}}(\gamma_s) = \Pr[\gamma_{psr}^{\mathrm{AF}} < \gamma_s]$ can be expressed using (9) as

$$F_{\gamma_{psr}^{\mathrm{AF}}}(\gamma_s) = \Pr\left[\frac{(1-\zeta)\gamma_{ps}\beta|h_{sr}|^2}{\zeta\beta|h_{sr}|^2 + \zeta\beta\gamma_{ps}|h_R|^2 + 1} < \gamma_s\right] = \Pr\left[\gamma_{ps} < \frac{\gamma_s(1+\zeta\beta|h_{sr}|^2)}{|h_{sr}|^2\beta T_1 - \zeta\beta\gamma_s|h_R|^2}\right], \tag{71}$$

which can be further evaluated as

$$F_{\gamma_{psr}^{\mathrm{AF}}}(\gamma_s) = \int_0^\infty\left(\int_{\frac{\zeta\gamma_s z}{T_1}}^\infty\left(\int_0^{\frac{\gamma_s(1+\zeta\beta y)}{T_1\beta y-\zeta\beta\gamma_s z}} f_{\gamma_{ps}}(x)dx\right)f_{|h_{sr}|^2}(y)dy\right) \times f_{|h_R|^2}(z)dz. \tag{72}$$

Now, by substituting the PDF $f_{\gamma_{ps}}(x)$ and then solving the associated integral, (72) can be simplified as

$$F_{\gamma_{psr}^{\mathrm{AF}}}(\gamma_s) = \int_0^\infty\left(\int_{\frac{\zeta\gamma_s z}{T_1}}^\infty\left(1 - \sum_{k=0}^{m_{ps}-1}\frac{(T_0\gamma_s)^k}{k!}e^{-\left(\frac{T_0\gamma_s(1+\zeta\beta y)}{T_1 y-\zeta\gamma_s z}\right)} \times\left(\frac{1+\zeta\beta y}{T_1 y-\zeta\gamma_s z}\right)^k\right)f_{|h_{sr}|^2}(y)dy\right) \times f_{|h_R|^2}(z)dz. \tag{73}$$

Hereby, (73) can be represented as $F_{\gamma_{psr}^{\mathrm{AF}}}(\gamma_s) = \Psi_1(\gamma_s) - \Psi_2(\gamma_s)$, with $\Psi_1(\gamma_s)$ given by

$$\Psi_1(\gamma_s) = \int_0^\infty\left(\int_{\frac{\zeta\gamma_s z}{T_1}}^\infty f_{|h_{sr}|^2}(y)dy\right)f_{|h_R|^2}(z)dz. \tag{74}$$

After inserting the associated PDF expressions of y and z into (74) and simplifying further, one can arrive at (50). Next, we focus on the evaluation of $\Psi_2(\gamma_s)$, which can be written while following (73) as

$$\Psi_2(\gamma_s) = \int_0^\infty\left(\int_{\frac{\zeta\gamma_s z}{T_1}}^\infty\left(\sum_{k=0}^{m_{ps}-1}\frac{(T_0\gamma_s)^k}{k!}e^{-\left(\frac{T_0\gamma_s(1+\zeta\beta y)}{T_1 y-\zeta\gamma_s z}\right)} \times\left(\frac{1+\zeta\beta y}{T_1 y-\zeta\gamma_s z}\right)^k\right)f_{|h_{sr}|^2}(y)dy\right) \times f_{|h_R|^2}(z)dz. \tag{75}$$

Now, invoking the PDF expression $f_{|h_{sr}|^2}(y)$ along with a substitution $T_1 y - \zeta\gamma_s z = t$, $\Psi_2(\gamma_s)$ can be re-expressed as

$$\Psi_2(\gamma_s) = \int_0^\infty\left(\mathbb{M}\int_0^\infty t^{m-k}e^{-\frac{T_0\gamma_s(\zeta^2\beta\gamma_s z+T_1)}{T_1 t}-\frac{m_{sr}}{\Omega_{sr}T_1}t}dt\right) z^{j+m_{sr}-1-m}e^{-T_2\zeta z}f_{|h_R|^2}(z)dz, \tag{76}$$

where

$$\mathbb{M} = \sum_{k=0}^{m_{ps}-1}\sum_{j=0}^{k}\sum_{m=0}^{j+m_{sr}-1}\frac{(T_0\gamma_s)^k}{k!}\frac{1}{\Gamma(m_{sr})}\left(\frac{m_{sr}}{\Omega_{sr}}\right)^{m_{sr}}\binom{k}{j}(\zeta\beta)^j \times\left(\frac{1}{T_1}\right)^{j+m_{sr}}\binom{j+m_{sr}-1}{m}(\zeta\gamma_s)^{j+m_{sr}-1-m}e^{\frac{-T_0\gamma_s\zeta\beta}{T_1}}. \tag{77}$$

On computing the inner integral in (76) using [43, eq. (3.471.9)], and then simplifying while substituting the PDF expression $f_{|h_R|^2}(z)$, $\Psi_2(\gamma_s)$ can be obtained as

$$\Psi_2(\gamma_s) = \mathbb{M} \times \frac{1}{\Gamma(m_R)}\left(\frac{m_R}{\Omega_R}\right)^{m_R}\int_0^\infty z^{j+m_R+m_{sr}-2-m} \times e^{\left(-T_2\zeta z-\frac{m_R}{\Omega_R}z\right)}2\left(\frac{T_0\gamma_s\Omega_{sr}\left(T_1+\zeta^2\beta\gamma_s z\right)}{m_{sr}}\right)^{\frac{m-k+1}{2}} \times \mathcal{K}_{m-k+1}\left(2\sqrt{\frac{T_0\gamma_s m_{sr}\left(T_1+\zeta^2\beta\gamma_s z\right)}{\Omega_{sr}T_1^2}}\right)dz. \quad (78)$$

Finally, substituting $(T_1+\zeta^2\beta\gamma_s z)=\theta$ into (78), and simplifying further, one can get the required result as provided in (51).

APPENDIX C

Using (18), the CDF $F_{\gamma_{sr}^{\text{noc}}}(\gamma_s) = \Pr[\gamma_{sr}^{\text{noc}} < \gamma_s]$ can be expressed as

$$F_{\gamma_{sr}^{\text{noc}}}(\gamma_s) = \Pr\left[\beta\gamma_{ps}|h_{sr}|^2 < \gamma_s\right] = \Pr\left[|h_{sr}|^2 < \frac{\gamma_s}{\beta\gamma_{ps}}\right], \quad (79)$$

which can be further evaluated as

$$F_{\gamma_{sr}^{\text{noc}}}(\gamma_s) = \int_0^\infty F_{|h_{sr}|^2}\left(\frac{\gamma_s}{\beta\gamma_{ps}}\right)f_{\gamma_{ps}}(y)dy. \quad (80)$$

On substituting the corresponding PDF, CDF in (80) and simplifying further with the aid of [43, eq. (3.351.3)], one can get the required result as provided in (53).

APPENDIX D

From (57), the probability term P_{12} can be expressed as

$$P_{12} = \Pr\left[|h_{sr}|^2 < \frac{\gamma_s}{\beta\gamma_{ps}^{\text{DL}}},\ |h_{sr}|^2 \geq \frac{\gamma_s}{\beta\gamma_p}\right], \quad (81)$$

which can be further evaluated as

$$P_{12} = \int_0^\infty\left(\int_{\frac{\gamma_s}{\beta\gamma_p}}^{\frac{\gamma_s}{\beta\eta_p z}} f_{|h_{sr}|^2}(y)dy\right)f_{\gamma_{ps}^{\text{DL}}}(z)dz = \int_0^\infty F_{|h_{sr}|^2}\left(\frac{\gamma_s}{\beta\eta_p z}\right)f_{\gamma_{ps}^{\text{DL}}}(z)dz - \int_0^\infty F_{|h_{sr}|^2}\left(\frac{\gamma_s}{\beta\gamma_p}\right)f_{\gamma_{ps}^{\text{DL}}}(z)dz. \quad (82)$$

On substituting the corresponding PDF and CDF in (82) and simplifying further with the aid of [43, eq. (3.351.3)], one can obtain the desired result as given in (59).

REFERENCES

[1] S. Lee, R. Zhang, and K. Huang, "Opportunistic wireless energy harvesting in cognitive radio networks," *IEEE Trans. Wireless Commun.*, vol. 12, no. 9, pp. 4788–4799, Sep. 2013.

[2] L. Dai, B. Wang, Y. Yuan, S. Han, I. Chih-Lin, and Z. Wang, "Non-orthogonal multiple access for 5G: Solutions, challenges, opportunities, and future research trends," *IEEE Commun. Mag.*, vol. 53, no. 9, pp. 74–81, Sep. 2015.

[3] S. M. R. Islam, N. Avazov, O. A. Dobre, and K.-S. Kwak, "Power-domain non-orthogonal multiple access (NOMA) in 5G systems: Potentials and challenges," *IEEE Commun. Surveys Tuts.*, vol. 19, no. 2, pp. 721–742, 2nd Quart., 2017.

[4] Z. Ding, X. Lei, G. K. Karagiannidis, R. Schober, J. Yuan, and V. K. Bhargava, "A survey on non-orthogonal multiple access for 5G networks: Research challenges and future trends," *IEEE J. Sel. Areas Commun.*, vol. 35, no. 10, pp. 2181–2195, Oct. 2017.

[5] Z. Wei, L. Yang, D. W. K. Ng, J. Yuan, and L. Hanzo, "On the performance gain of NOMA over OMA in uplink communication systems," *IEEE Trans. Commun.*, vol. 68, no. 1, pp. 536–568, Jan. 2020.

[6] D. Tse and P. Viswanath, *Fundamentals of Wireless Communication*, Cambridge, U.K.: Cambridge Univ. Press, 2005.

[7] Z. Ding, Z. Yang, P. Fan, and H. V. Poor, "On the performance of non-orthogonal multiple access in 5G systems with randomly deployed users," *IEEE Signal Process. Lett.*, vol. 21, no. 12, pp. 1501–1505, Dec. 2014.

[8] Z. Ding, P. Fan, and H. V. Poor, "Impact of user pairing on 5G nonorthogonal multiple-access downlink transmissions," *IEEE Trans. Veh. Technol.*, vol. 65, no. 8, pp. 6010–6023, Aug. 2016.

[9] S. Haykin, "Cognitive radio: Brain-empowered wireless communications," *IEEE J. Sel. Areas Commun.*, vol. 23, no. 2, pp. 201–220, Feb. 2005.

[10] A. Goldsmith, S. A. Jafar, I. Maric, and S. Srinivasa, "Breaking spectrum gridlock with cognitive radios: An information theoretic perspective," *Proc. IEEE*, vol. 97, no. 5, pp. 894–914, May 2009.

[11] H. A. Suraweera, P. J. Smith, and M. Shafi, "Capacity limits and performance analysis of cognitive radio with imperfect channel knowledge," *IEEE Trans. Veh. Technol.*, vol. 59, no. 4, pp. 1811–1822, May 2010.

[12] Y. Han, A. Pandharipande, and S. H. Ting, "Cooperative decode-and-forward relaying for secondary spectrum access," *IEEE Trans. Wireless Commun.*, vol. 8, no. 10, pp. 4945–4950, Oct. 2009.

[13] S. Macdonald, D. C. Popescu, and O. Popescu, "A hybrid framework for spectrum sharing in cognitive radio systems with dynamic users," *IEEE Commun. Lett.*, vol. 23, no. 10, pp. 1871–1874, Oct. 2019.

[14] L. Lv, J. Chen, Q. Ni, Z. Ding, and H. Jiang, "Cognitive non-orthogonal multiple access with cooperative relaying: A new wireless frontier for 5G spectrum sharing," *IEEE Commun. Mag.*, vol. 56, no. 4, pp. 188–195, Apr. 2018.

[15] Y. Liu, Z. Ding, M. Elkashlan, and J. Yuan, "Nonorthogonal multiple access in large-scale underlay cognitive radio networks," *IEEE Trans. Veh. Technol.*, vol. 65, no. 12, pp. 10152–10157, Dec. 2016.

[16] S. Arzykulov, G. Nauryzbayev, T. A. Tsiftsis, and B. Maham, "Performance analysis of underlay cognitive radio nonorthogonal multiple access networks," *IEEE Trans. Veh. Technol.*, vol. 68, no. 9, pp. 9318–9322, Sep. 2019.

[17] S. Arzykulov, G. Nauryzbayev, T. A. Tsiftsis, B. Maham, and M. Abdallah, "On the outage of underlay CR-NOMA networks with detect-and-forward relaying," *IEEE Trans. Cogn. Commun. Netw.*, vol. 5, no. 3, pp. 795–804, Sep. 2019.

[18] K. Sultan, "Best relay selection schemes for NOMA based cognitive relay networks in underlay spectrum sharing," *IEEE Access*, vol. 8, pp. 190160–190172, 2020.

[19] T.-T. Nguyen, T.-H. Vu, T.-V. Nguyen, D. B. da Costa, and C. D. Ho, "Underlay cognitive NOMA-based coordinated direct and relay transmission," *IEEE Wireless Commun. Lett.*, vol. 10, no. 4, pp. 854–858, Apr. 2021.

[20] L. Lv, Q. Ni, Z. Ding, and J. Chen, "Application of non-orthogonal multiple access in cooperative spectrum-sharing networks over Nakagami-*m* fading channels," *IEEE Trans. Veh. Technol.*, vol. 66, no. 6, pp. 5510–5515, Jun. 2017.

[21] L. Lv, L. Yang, H. Jiang, T. H. Luan, and J. Chen, "When NOMA meets multiuser cognitive radio: Opportunistic cooperation and user scheduling," *IEEE Trans. Veh. Technol.*, vol. 67, no. 7, pp. 6679–6684, Jul. 2018.

[22] L. Luo, Q. Li, and J. Cheng, "Performance analysis of overlay cognitive NOMA systems with imperfect successive interference cancellation," *IEEE Trans. Commun.*, vol. 68, no. 8, pp. 4709–4722, Aug. 2020.

[23] M. F. Kader, "A power-domain NOMA based overlay spectrum sharing scheme," *Future Gener. Comput. Syst.*, vol. 105, pp. 222–229, Apr. 2020.

[24] V. Singh, P. K. Upadhyay, and M. Lin, "On the performance of NOMA-assisted overlay multiuser cognitive satellite-terrestrial networks," *IEEE Wireless Commun. Lett.*, vol. 9, no. 5, pp. 638–642, May 2020.

[25] S. Singh and M. Bansal, "Performance analysis of NOMA-based AF cooperative overlay system with imperfect CSI and SIC," *IEEE Access*, vol. 9, pp. 40263–40273, 2021.

[26] X. Huang, T. Han, and N. Ansari, "On green-energy-powered cognitive radio networks," *IEEE Commun. Surveys Tuts.*, vol. 17, no. 2, pp. 827–842, 2nd Quart., 2015.

[27] X. Lu, P. Wang, D. Niyato, D. I. Kim, and Z. Han, "Wireless networks with RF energy harvesting: A contemporary survey," *IEEE Commun. Surveys Tuts.*, vol. 17, no. 2, pp. 757–789, 2nd Quart., 2015.

[28] I. Krikidis, S. Timotheou, S. Nikolaou, G. Zheng, D. W. K. Ng, and R. Schober, "Simultaneous wireless information and power transfer in modern communication systems," *IEEE Commun. Mag.*, vol. 52, no. 11, pp. 104–110, Nov. 2014.

[29] L. R. Varshney, "Transporting information and energy simultaneously," in *Proc. IEEE Int. Symp. Inf. Theory (ISIT)*, Toronto, ON, Canada, Jul. 2008, pp. 1612–1616.

[30] X. Zhou, R. Zhang, and C. K. Ho, "Wireless information and power transfer: Architecture design and rate-energy tradeoff," *IEEE Trans. Commun.*, vol. 61, no. 11, pp. 4754–4767, Nov. 2013.

[31] S. Solanki, P. K. Upadhyay, D. B. da Costa, H. Ding, and J. M. Moualeau, "Performance analysis of piece-wise linear model of energy harvesting-based multiuser overlay spectrum sharing networks," *IEEE Open J. Commun. Soc.*, vol. 1, pp. 1820–1836, 2020.

[32] Y. Xu *et al.*, "Joint beamforming and power-splitting control in downlink cooperative SWIPT NOMA systems," *IEEE Trans. Signal Process.*, vol. 65, no. 18, pp. 4874–4886, Sep. 2017.

[33] D. Wang and S. Men, "Secure energy efficiency for NOMA based cognitive radio networks with nonlinear energy harvesting," *IEEE Access*, vol. 6, pp. 62707–62716, 2018.

[34] F. Li, H. Jiang, R. Fan, and P. Tan, "Cognitive non-orthogonal multiple access with energy harvesting: An optimal resource allocation approach," *IEEE Trans. Veh. Technol.*, vol. 68, no. 7, pp. 7080–7095, Jul. 2019.

[35] X. Wang *et al.*, "Energy efficiency optimization for NOMA-based cognitive radio with energy harvesting," *IEEE Access*, vol. 7, pp. 139172–139180, 2019.

[36] Y. Yu, Z. Yang, Y. Wu, J. A. Hussein, W.-K. Jia, and Z. Dong, "Outage performance of NOMA in cooperative cognitive radio networks with SWIPT," *IEEE Access*, vol. 7, pp. 117308–117317, 2019.

[37] T.-H. Vu and S. Kim, "Performance evaluation of power beacon-assisted wireless powered NOMA IoT-based systems," *IEEE Internet Things J.*, early access, Feb. 11, 2021, doi: 10.1109/JIOT.2021.3058680.

[38] X. Yue, Y. Liu, Y. Yao, X. Li, R. Liu, and A. Nallanathan, "Secure communications in a unified non-orthogonal multiple access framework," *IEEE Trans. Wireless Commun.*, vol. 19, no. 3, pp. 2163–2178, Mar. 2020.

[39] N. S. Mouni, A. Kumar, and P. K. Upadhyay, "Adaptive user pairing for NOMA systems with imperfect SIC," *IEEE Wireless Commun. Lett.*, early access, Apr. 19, 2021, doi: 10.1109/LWC.2021.3074036.

[40] G. Im and J. H. Lee, "Outage probability for cooperative NOMA systems with imperfect SIC in cognitive radio networks," *IEEE Commun. Lett.*, vol. 23, no. 4, pp. 692–695, Apr. 2019.

[41] K.-G. Nguyen, Q.-D. Vu, L.-N. Tran, and M. Juntti, "Energy efficiency fairness for multi-pair wireless-powered relaying systems," *IEEE J. Sel. Areas Commun.*, vol. 37, no. 2, pp. 357–373, Feb. 2019.

[42] P. Kumar and K. Dhaka, "Performance of wireless powered DF relay system under Nakagami-*m* fading: Relay assists energy-constrained source," *IEEE Syst. J.*, vol. 14, no. 2, pp. 2497–2507, Jun. 2020.

[43] I. S. Gradshteyn and I. M. Ryzhik, *Tables of Integrals, Series and Products*, 6th ed. New York, NY, USA: Academic, 2000.

[44] A. A. Nasir, X. Zhou, S. Durrani, and R. A. Kennedy, "Relaying protocols for wireless energy harvesting and information processing," *IEEE Trans. Wireless Commun.*, vol. 12, no. 7, pp. 3622–3636, Jul. 2013.

[45] E. Boshkovska, D. W. K. Ng, N. Zlatanov, and R. Schober, "Practical non-linear energy harvesting model and resource allocation for SWIPT systems," *IEEE Commun. Lett.*, vol. 19, no. 12, pp. 2082–2085, Dec. 2015.

[46] A. Kumar and K. Kumar, "Relay sharing with DF and AF techniques in NOMA assisted cognitive radio networks," *Phys. Commun.*, vol. 42, Oct. 2020, Art. no. 101143.

[47] D. S. Gurjar, U. Singh, and P. K. Upadhyay, "Energy harvesting in hybrid two-way relaying with direct link under Nakagami-*m* fading," in *Proc. IEEE Wireless Commun. Netw. Conf. (WCNC)*, Barcelona, Spain, Apr. 2018, pp. 1–6.

[48] V. Aswathi and A. V. Babu, "Full/half duplex cooperative NOMA under imperfect successive interference cancellation and channel state estimation errors," *IEEE Access*, vol. 7, pp. 179961–179984, 2019.

[49] N. B. Mehta, V. Sharma, and G. Bansal, "Performance analysis of a cooperative system with rateless codes and buffered relays," *IEEE Trans. Wireless Commun.*, vol. 10, no. 4, pp. 1069–1081, Apr. 2011.

[50] I. Stanojev, O. Simeone, Y. Bar-Ness, and C. You, "Performance of multi-relay collaborative hybrid-ARQ protocols over fading channels," *IEEE Commun. Lett.*, vol. 10, no. 7, pp. 522–524, Jul. 2006.

[51] V. A. Aalo and J. Zhang, "Performance analysis of maximal ratio combining in the presence of multiple equal-power cochannel interferers in a Nakagami fading channel," *IEEE Trans. Veh. Technol.*, vol. 50, no. 2, pp. 497–503, Mar. 2001.

[52] T. M. Hoang, B. C. Nguyen, P. T. Tran, and L. T. Dung, "Outage analysis of RF energy harvesting cooperative communication systems over Nakagami-*m* fading channels with integer and non-integer *m*," *IEEE Trans. Veh. Technol.*, vol. 69, no. 3, pp. 2785–2801, Mar. 2020.

[53] C. Zhang, J. Ge, J. Li, Y. Rui, and M. Guizani, "A unified approach for calculating the outage performance of two-way AF relaying over fading channels," *IEEE Trans. Veh. Technol.*, vol. 64, no. 3, pp. 1218–1229, Mar. 2015.

[54] Y. Liu, L. Wang, M. Elkashlan, T. Q. Duong, and A. Nallanathan, "Two-way relay networks with wireless power transfer: Design and performance analysis," *IET Commun.*, vol. 10, no. 14, pp. 1810–1819, Jun. 2016.

[55] S. Solanki, V. Singh, and P. K. Upadhyay, "RF energy harvesting in hybrid two-way relaying systems with hardware impairments," *IEEE Trans. Veh. Technol.*, vol. 68, no. 12, pp. 11792–11805, Dec. 2019.

[56] L. Liu, R. Zhang, and K.-C. Chua, "Wireless information and power transfer: A dynamic power splitting approach," *IEEE Trans. Commun.*, vol. 61, no. 9, pp. 3990–4001, Sep. 2013.

[57] D. Wang, F. Rezaei, and C. Tellambura, "Performance analysis and resource allocations for a WPCN with a new nonlinear energy harvester model," *IEEE Open J. Commun. Soc.*, vol. 1, pp. 1403–1424, 2020.

ALOK KUMAR SHUKLA (Graduate Student Member, IEEE) received the B.E. degree in electronics and communication engineering, and the M.E. degree in digital communication from Rajiv Gandhi Proudyogiki Vishwavidyalaya, Bhopal, India, in 2015 and 2018, respectively. He is currently pursuing the Ph.D. degree in electrical engineering with the Indian Institute of Technology Indore, Indore, India. His research interests include wireless body area network, energy harvesting, cognitive radio, and non-orthogonal multiple access schemes.

VIBHUM SINGH (Graduate Student Member, IEEE) received the B.Tech. degree in electronics and communication engineering from Uttar Pradesh Technical University, Lucknow, India, in 2011, and the M.Tech. degree in telecommunication systems engineering from the Indian Institute of Technology (IIT) Kharagpur, Kharagpur, India, in 2015. He is currently pursuing the Ph.D. degree in electrical engineering with IIT Indore, Indore, India. His main research interests are in hybrid satellite-terrestrial systems, cognitive radio, wireless energy harvesting, and NOMA. He was a recipient of the Student Travel Grant for the IEEE Wireless Communications and Networking Conference, Seoul, South Korea, in 2020. He has been involved in peer review process of major IEEE journals and conferences. He is a member of IEEE Communication Society and IEEE Young Professionals.

PRABHAT K. UPADHYAY (Senior Member, IEEE) received the Ph.D. degree in electrical engineering from the Indian Institute of Technology (IIT) Delhi, New Delhi, India, in 2011. He was a Lecturer with the Department of Electronics and Communication Engineering, Birla Institute of Technology Mesra, Ranchi. He joined IIT Indore as an Assistant Professor of Electrical Engineering, in 2012, where he has been an Associate Professor, since 2017. He has also led various research projects in the Wireless Communications Research Group, IIT Indore. He has numerous publications in peer-reviewed journals and conferences and has authored a book and six book chapters. His main research interests include wireless relaying techniques, cooperative communications, MIMO signal processing, hybrid satellite-terrestrial systems, cognitive radio, and molecular communications. He has been awarded the Sir Visvesvaraya Young Faculty Research Fellowship under the Ministry of Electronics and Information Technology, Government of India, and the IETE-Prof SVC Aiya Memorial Award 2018. He was a co-recipient of the Best Paper Award at the International Conference on Advanced Communication Technologies and Networking, Marrakech, Morocco, in 2018. He has served as a Guest Editor of the Special Issue on Energy-Harvesting Cognitive Radio Networks in the IEEE TRANSACTIONS ON COGNITIVE COMMUNICATIONS AND NETWORKING and is currently serving as an Editor of the IEEE COMMUNICATIONS LETTERS, IEEE ACCESS, and *Frontiers in Communications and Networks*. He has been involved in technical program committee of several premier conferences. He is a member of the IEEE Communications Society and the IEEE Vehicular Technology Society, and a Life Member of the Institution of Electronics and Telecommunication Engineers.

ABHINAV KUMAR (Senior Member, IEEE) received the dual B.Tech. and M.Tech. degrees and Ph.D. degree from the Indian Institute of Technology Delhi, New Delhi, India, in 2009 and 2013, respectively. He has worked as a Postdoctoral Fellow with the University of Waterloo, Canada, from 2013 to 2014. Since November 2014, he has been with the Indian Institute of Technology Hyderabad, Hyderabad, India, where he is currently an Associate Professor. His research interests are in the various aspects of wireless communications and networking including energy efficiency, visible light based communications, cellular IoT, resource allocation, and multiple access techniques for heterogeneous networks.

JULES M. MOUALEU (Senior Member, IEEE) received the Ph.D. degree in electronic engineering from the University of KwaZulu–Natal, Durban, South Africa, in 2013. During his Ph.D. studies, he was a Visiting Scholar with Concordia University, Montreal, QC, Canada, under the Canadian Commonwealth Scholarship Program offered by the Foreign Affairs and International Trade Canada. In 2015, He joined the Department of Electrical and Information Engineering, University of the Witwatersrand, Johannesburg, South Africa, where he is currently an Associate Professor. From 2018 to 2021, he was an Affiliate Assistant Professor with Concordia University. He is currently an NRF Y-Rated Researcher. His current research interests include cooperative and relay communications, wireless body area networks, energy harvesting, massive multiple-input multiple-output systems, non-orthogonal multiple access schemes, and physical-layer security. He received the Exemplary Reviewer Award of the IEEE COMMUNICATIONS LETTERS in 2018, 2019, and 2020. He currently serves as an Associate Editor of IEEE ACCESS and *Frontiers in Communications and Networks*.